UNIVERSIDADE FEDERAL DE SANTA CATARINA

CAMPUS TRINDADE

PROGRAMA DE PÓS-GRADUAÇÃO EM ENGENHARIA MECÂNICA

Michel Batista Siqueira

Wire electrical discharge machining of Nd-Fe-B magnets

Florianópolis

2023

Michel Batista Siqueira

Wire electrical discharge machining of Nd-Fe-B magnets

Dissertação submetida ao Programa de Pós-Graduação em Engenharia Mecânica da Universidade Federal de Santa Catarina para a obtenção do título de Mestre em Engenharia Mecânica.

Orientador: Prof. Fabio Antonio Xavier, Dr. Eng.
Coorientador: Prof. Leonardo Ulian Lopes, Dr. Eng,

Florianópolis
2023

Michel Batista Siqueira

Wire electrical discharge machining of Nd-Fe-B Magnets

O presente trabalho em nível de mestrado foi avaliado e aprovado por banca examinadora composta pelos seguintes membros:

Prof. Dr. Eng. Milton Pereira

Universidade Federal de Santa Catarina - UFSC

Profa. Dra. Cristiani Campos Plá Cid

Universidade Federal de Santa Catarina - UFSC

Certificamos que esta é a **versão original e final** do trabalho de conclusão que foi julgado adequado para obtenção do título de Mestre em Engenharia Mecânica.

Documento assinado digitalmente
Henrique Simas
Data: 26/01/2024 15:13:41-0300
CPF: ***.194.639-**
Verifique as assinaturas em https://v.ufsc.br

Coordenação do Programa de Pós-Graduação.

Documento assinado digitalmente
Fabio Antonio Xavier
Data: 09/01/2024 08:43:57-0300
CPF: ***.591.289-**
Verifique as assinaturas em https://v.ufsc.br

Prof. Dr. Eng. Fabio Antonio Xavier – Orientador

Universidade Federal de Santa Catarina – UFSC

Florianópolis, 2023.

Ficha de identificação da obra elaborada pelo autor,
através do Programa de Geração Automática da Biblioteca Universitária da UFSC.

Batista Siqueira, Michel
Wire electrical discharge machining of Nd-Fe-B magnets / Michel Batista Siqueira ; orientador, Fabio Antonio Xavier, coorientador, Leonardo Ulian, 2023.
91 p.

Dissertação (mestrado) - Universidade Federal de Santa Catarina, Centro Tecnológico, Programa de Pós-Graduação em Engenharia Mecânica, Florianópolis, 2023.

Inclui referências.

1. Engenharia Mecânica. 2. eletroerosao. 3. eletroerosao a fio. 4. ímas de Nd-Fe-B. I. Xavier, Fabio Antonio. II. Ulian, Leonardo. III. Universidade Federal de Santa Catarina. Programa de Pós-Graduação em Engenharia Mecânica. IV. Título.

Dedico este trabalho ao Criador.

AGRADECIMENTOS

Gostaria de expressar meus sinceros agradecimentos, primeiramente a Deus, pela oportunidade concedida para realizar este trabalho de mestrado com excelência. Quero também expressar minha profunda gratidão aos meus pais, minha avó, meus irmãos, familiares e amigos, que sempre me apoiaram incondicionalmente ao longo dessa jornada. Suas palavras de encorajamento e apoio foram fundamentais para o meu sucesso.

Gostaria de aproveitar esta oportunidade para expressar minha gratidão ao meu orientador, Professor Fábio Antônio Xavier, que sempre me apoiou, acreditou em meu potencial e me motivou a seguir em frente durante todo o desenvolvimento deste trabalho. Sua orientação foi essencial para minha formação acadêmica e profissional. Também sou grato ao meu co-orientador, Professor Leonardo Ulian, por sua valiosa contribuição no entendimento de materiais magnéticos e por suas orientações precisas nos experimentos realizados nessa área.

Gostaria de expressar minha gratidão ao Professor Rolf Schroeter por seus sábios conselhos, ao Professor Walter Weingaertner por me ajudar a esclarecer várias dúvidas, desde questões relacionadas a elétrons até informações sobre os sumérios. Agradeço também ao Professor Paulo Wendhausen por me proporcionar a oportunidade de aprender mais sobre a fabricação de ímãs de terras-raras, bem como à Professora Deise Schafer pela permissão e pelo treinamento na utilização dos equipamentos de caracterização magnética.

Não posso deixar de agradecer aos parceiros de outros laboratórios que tornaram possível a realização deste trabalho, por meio da permissão para utilizar seus equipamentos. Gostaria de expressar minha sincera gratidão ao excelente profissional Charles Nuernberg, por toda a ajuda e permissão para utilizar os equipamentos do IFSC, mesmo durante períodos festivos. Agradeço também ao técnico Gleizer pelo apoio nas caracterizações magnéticas e à Doutora Patrícia pelo suporte com a microscopia eletrônica de varredura.

Quero agradecer aos amigos que fiz ao longo da minha trajetória como mestrando, tanto no Laboratório de Precisão Mecânica quanto nas outras pessoas que conheci em diferentes laboratórios e instituições, e que me ajudaram ao longo desse caminho desafiador.

Não poderia deixar de expressar minha gratidão ao POSMEC por ter me aceitado no programa de mestrado, assim como à UFSC e à CAPES pelo incentivo e apoio à pesquisa.

Mais uma vez, gostaria de agradecer a todos os mencionados, bem como a todos aqueles que contribuíram direta ou indiretamente para o meu sucesso neste trabalho de mestrado. Seu apoio e encorajamento foram inestimáveis e sou profundamente grato por tê-los ao meu lado ao longo dessa jornada. Desejo a todos sucesso contínuo em suas trajetórias acadêmicas e profissionais, e que possamos continuar a compartilhar experiências e conhecimento no campo da pesquisa.

Non solus.

ABSTRACT

Neodymium-iron-boron (Nd-Fe-B) magnets were first sintered in the early 1980s. They are known for their applications in technologies such as wind turbines, electric cars and hard drives. This material presents brittle behavior, which makes its machinability difficult by conventional methods such as turning and milling. In this context, the machining aspects of this material with unconventional methods such as electrical discharge machining (EDM) became relevant. The aim of this study is to understand how the variation of EDM machining parameters influences the results of surface integrity, roughness and magnetic properties of Nd-Fe-B magnets. A Nd-Fe-B wind turbine magnet block was machined into samples by the wire electrical discharge machining (WEDM) process. This wind turbine block was machined with an AgieCut Challenge machine from the manufacturer Charmilles using a molybdenum wire with a diameter of 0.18 mm. Based on the literature and the available parameters of the machine, four cutting conditions were chosen: roughing, semi-finishing and two finishing conditions. After the machining, the surface roughness, surface morphology, chemical composition, coercivity and remanence of the samples were analyzed. The resulting roughness for each cutting condition was characterized with a Taylor Surf rugosimeter, Form TaylorSurf il20 model and the data for all samples treated with MountainView software. To evaluate the surface morphology, chemical element map and cross section, optical microscopy (OM), scanning electron microscopy (SEM) and energy dispersive spectroscopy (EDS) techniques were used. The results showed that a phenomenon of spheroidization of the machined material occurred mainly for the roughing condition, where a layer of remelted material in the form of spheres was not removed by the dielectric and was stuck on the surface of the material. This layer of spheres caused a considerable increase in the roughness values and also a significant detrimental effect in the magnetic properties of the samples, when compared with the samples machined by the semi-finishing and finishing conditions. Based on the analysis, the following conclusions could be drawn from this work: although the WEDM process is indicated for Nd-Fe-B machining, the use of post-processing is necessary to eliminate the layer of remelted material that remains on the surface, which has an impact on the magnetic properties of the magnets with a reduction of 30% in coercivity and 27% and remanence for magnets machined by rough machining when compared to finishing machining.

Keywords: Wire electrical discharge machining, rare-earth magnets, EDM, Nd-Fe-B.

FIGURES LIST

TABLES LIST

ACRONYMS LIST

REEs – Rare-earth elements

UFSC –Federal University of Santa Catarina;

IFSC – Federal Institute of Santa Catarina;

LMP – Machining Precision Laboratory;

MAGMA – Magnetic Materials Group

LabMat – Materials Laboratory;

REGINA – Rare Earth Global Industry and New Applications;

DIN – Deutsch Institut für Normung

ISO – International Organization for Standardization;

USGS – United States Geological Survey;

EDM – Electrical discharge machining;

WEDM – Wire electrical discharge machining;

SEM – Scanning electron microscopy;

EDS – Energy dispersive spectroscopy;

BSE – Back-scattered electron;

SE – Secondary electron;

OM – Optical Microscope;

HD – Hydrogen Decreptation;

RMS – Root mean square;

VSM – Vibrating sample magnetometer;

SYMBOLS LIST

R_a – Average roughness;

R_q – Root mean square roughness

R_t – Total height of the profile;

R_z – Maximum height of the profile;

Fe – Iron;

Mo – Molybdenum;

C – Carbon;

O – Oxygen;

B – Boron;

Nd – Neodymium;

Pr – Praseodymium;

Dy – Dysprosium;

Al – Aluminum;

H_cJ – Coercivity;

B_r – Remanence;

$(BH)_{Max}$ – Maximum product energy;

Nd-Rich – Neodymium rich phase;

IP – Peak current;

SUMMARY

RESUMO EXPANDIDO EM PORTUGUÊS

Introdução

O processo de corte por descargas elétricas ou eletroerosão é amplamente utilizado para operações de usinagem em que a precisão e a geometria complexa do corte são importantes requisitos de projeto. Na fabricação de ímãs condutores, este processo é empregado para cortar os blocos sinterizados de ligas magnéticas. Uma dessas ligas é composta majoritariamente de neodímio, ferro e boro. Ímãs de neodímio-ferro-boro (Nd-Fe-B) são amplamente utilizados devido ao seu alto valor de produto de energia em tecnologias como turbinas eólicas, carros elétricos e discos rígidos. Este material apresenta comportamento quebradiço e frágil, o que dificulta sua usinagem por métodos convencionais como torneamento, serramento e fresamento. Nesse contexto, tornaram-se relevantes os aspectos de usinagem desse material através de métodos não convencionais, como a usinagem por descargas elétricas, do inglês, *electrical discharge machining (EDM)*. O presente trabalho tem como objetivo entender melhor como os parâmetros de eletroerosão a fio afetam a rugosidade, integridade da superfície e propriedades magnéticas de amostras de Nd-Fe-B obtidas a partir de um bloco de ímã de aerogerador. As amostras foram usinadas em formato de paralelepípedos quadrados com lado de 5mm e altura de 250µm. Foram escolhidas quatro condições de corte, sendo uma delas classificada como desbaste, duas condições semelhantes classificadas como condições de semi-acabamento e uma condição de corte classificada como condição de acabamento de acordo com as especificações da máquina utilizada. O material do fio utilizado foi molibdênio e o dielétrico uma solução de óleo mineral e água destilada. As amostras com altura micrométrica foram caracterizadas com a utilização de rugosimetro, microscópio óptico, microscopia eletrônica de varredura e com magnetômetro de amostra vibrante. Os resultados obtidos foram utilizados nas caracterizações serviram para comparar o nível de dano que cada condição de corte causou nas amostras com relação a integridade de superfície e propriedades magnéticas como remanência e coercividade.

Objetivos

O objetivo principal deste estudo é avaliar a influência de diferentes condições de corte composta por diversos parâmetros de usinagem por descarga elétrica a fio na morfologia de superfície, rugosidade, subsuperfície e propriedades magnéticas de amostras usinadas com diferentes condições de corte. Nesse contexto, os objetivos específicos são apresentados a seguir:

• Investigar a superfície gerada por diferentes condições de corte através de microscopia óptica e microscopia eletrônica de varredura;

• Medir os parâmetros de rugosidade Ra, Rt, Rz e Rq para as diferentes condições de corte e correlacionar os resultados com as características de cada condição;

• Analisar de maneira geral a superfície e sub superfície com o auxílio de técnica de pré-polimento para seção transversal;

• Avaliar o impacto de diferentes condições de corte nas propriedades magnéticas das amostras através da análise das curvas de histerese, remanência e coercividade de micro ímãs de Nd-Fe-B usinados via WEDM e correlacionar com as alterações microestruturais

Metodologia

Um bloco de ímã de Nd-Fe-B de um aerogerador foi utilizado como material base para os experimentos. A direção de fácil magnetização do bloco é a direção da altura do bloco, sendo assim, as amostras de Nd-Fe-B foram usinadas por eletroerosão a fio a partir deste bloco, de maneira que as amostras possuíssem direção de fácil magnetização também na direção de sua altura. As amostras foram usinadas com quatro condições de cortes diferentes, sendo elas uma condição de desbaste, uma condição de semi-acabamento e duas condições de acabamento. A máquina utilizada foi uma máquina de eletroerosão a fio AgieCut Challenge FW1U, o eletrodo utilizado foi de molibdênio com 0,18 mm de diâmetro e o dielétrico uma emulsão de água e fluido dielétrico composto de óleo mineral com concentração de 20%. O primeiro passo foi caracterizar a rugosidade das amostras com auxílio de rugosímetro, em seguida a morfologia de superfície foi estudada com o auxílio de microscopia óptica e microscopia eletrônica de varredura. A técnica de espectroscopia por energia dispersiva também foi utilizada para inferir quantitativamente os elementos químicos presentes na superfície das amostras usinadas. Uma vez concluída a etapa de análise de superfície, foi realizada uma análise de secção transversal das amostras. Para tal, a metodologia de pré-polimento foi empregada. De maneira que as amostras foram polidas, posicionadas face-a-face com suas faces que estavam polidas e cortadas transversalmente a direção da face polida, de modo que fosse possível observar como a seção transversal foi impactada pelas diversas condições de corte. Por fim, as amostras foram caracterizadas em magnetômetro de amostra vibrante, onde suas propriedades de remanência e coercividade foram caracterizadas através do segundo quadrante da curva de histerese.

Resultados e discussão

Os resultados de rugosidade mostraram que a condição de desbaste produziu resultados de rugosidade média quatro vezes maiores em valor absoluto em relação à condição de semi-acabamento, e dez vezes maiores em relação às condições de acabamento. Com relação a morfologia de superfície, observou-se na condição de desbaste, a formação de uma camada composta por microesferas. Estas esferas apresentam composição química diferente entre elas, uma rica em neodímio e outra predominantemente composta de ferro livre. Tal fato indica que ocorreu refusão e formação de diferentes fases devido ao grande aporte energético proporcionado pelas descargas elétricas nesta condição de corte. Não foi observado nas superfícies usinadas pelas outras condições de corte mais brandas o mesmo fenômeno de formação de uma camada com microesferas. O que foi observado nesses casos foi a formação de uma camada de material refundido, e também a presença de cavacos esferoidizados, porém em tamanho e quantidade consideravelmente menores do que as superfícies usinadas pela primeira condição de corte. As análises de seção transversal mostraram que apesar de danificar significativamente a superfície, a subsuperfície não é afetada nem mesmo pela condição de corte mais agressiva. Os resultados de microscopia eletrônica de varredura e espectroscopia de energia dispersiva indicam que não houve impacto na fase primária $Nd_2Fe_{14}B$ na direção de profundidade do corte, mas que houve uma variação na profundidade afetada para cada diferente condição de corte. Os resultados de propriedades magnéticas mostraram que as amostras usinadas pela condição de corte mais agressiva sofreram um grande impacto em suas propriedades de coercividade e remanência, fato esse devido à liberação de ferro livre durante o processo de usinagem, que por ser considerado um material magneticamente mole, acabou impactando negativamente as propriedades magnéticas e curvas de histerese das amostras usinadas por eletroerosão a fio. As

condições de cortes mais brandas tiveram um efeito menor nas propriedades magnéticas das amostras analisadas. Entretanto, como a magnetização começa pela superfície, qualquer avaria na superfície possui um impacto no campo magnético e pode afetar significativamente o ciclo de histerese do material.

Considerações finais

Em geral, é possível concluir que a usinagem por descarga elétrica a fio é um processo de usinagem adequado para a fabricação de ímãs à base de terras-raras. Quanto mais agressiva a condição de corte, maiores serão os efeitos observados em sua superfície, e que, por sua vez, terá um efeito significativo nas propriedades magnéticas dos ímãs. Também foi observado que uma condição de corte muito agressiva provoca uma segregação de elementos químicos na superfície de ímãs de Nd-Fe-B, o que provoca um fenômeno de amolecimento magnético para as amostras usinadas por condições de corte agressivas e se intensifica conforme a relação superfície/volume da amostra aumenta. Apesar de o processo de eletroerosão a fio ser consideravelmente deletério para a superfície, não foi observada a presença de dano intenso na sub-superfície do material. A superfície dos ímãs de Neodímio-Ferro-Boro por sua vez ficou consideravelmente afetada para todas as condições de corte, fazendo-se necessário o uso de pós processamento na fabricação destes ímãs para aplicações de engenharia, pois a camada de material refundido e desproporcionado é prejudicial para as propriedades magnéticas.

1 - INTRODUCTION

The process of electrical discharge machining (EDM) is widely used for machining operations where the accuracy and complex cutting geometry are important design requirements. EDM is used for machining conductive materials, the electrode necessary for the discharge can have various types of forms like disk, cylindrical and wire. Wire-EDM is one process used in the manufacture of conductive magnets, this process is used to cut the sintered blocks of magnetic alloys. One of these alloys is mostly composed of neodymium, iron and boron. Neodymium-iron-boron (Nd-Fe-B) magnets are widely used because their high energy product value in technologies such as wind turbines, electric cars and hard disks. This material has brittle and fragile behavior, which makes it difficult for conventional machining methods such as turning, sawing and milling. In this context, the aspects of machining of this material with unconventional methods, such as electric discharge machining became relevant. This machining method is widely used in the manufacture of Nd-Fe-B magnets because its ability to generate complex geometries, and applications where high cutting accuracy is required. Nd-Fe-B magnets are known to present the highest maximum product-energy per unit of mass between the available magnets, being used whenever space and weight reduction are design requirements in power generation and electrical conversion machines [1]. Nd-Fe-B magnets are used in clean energy technologies such as wind turbine generators and hybrid or electric car batteries. As the demand for such technologies increases, the global rare-earth elements industry has taken steps such as increasing inventories, seeking to exploit economically viable deposits, and efforts to obtain efficient manufacturing and recycling routes for such elements [1,2]. In addition to the search for new mineral reserves for the exploration of REEs, a new source that began to be strongly considered from 2010 on is e-waste, especially in Japan, where it is estimated that there are about 300,000 tons of REEs in electronic products discarded [3].

Sintered rare-earth Neodymium Iron Boron magnets are typically produced by powder metallurgy and behave as hard and brittle material. Machining brittle materials, such as ceramics or certain types of glass, using

traditional machining processes like turning and sawing can be challenging and often impractical due to the intrinsic properties of these materials [4]. Because electrical discharge machining is a contactless thermal process, it is a widely known option when machining Nd-Fe-B magnets. Researchers reported a dramatic decrease in magnet flux density when these are subjected to highly aggressive rough machining conditions [5]. The literature needs information regarding the correlation of surface damage and impact on magnetic properties results for Nd-Fe-B magnets machined by wire electrical discharge machining. Since machining is an important step in the manufacturing of these magnets, a study on how the wire electrical discharge machining parameters influence the surface quality and magnetic properties is needed. Therefore, the present study conducted an evaluation on surface integrity and its correlation with magnetic properties for samples machined by wire electrical discharge machining in different conditions.

1.1 – RELEVANCE OF THEME

Brazil has a reserve of 22 thousand tons of economically viable REEs to be explored, having the second largest reserve after China [3]. In this context, a Brazil-Germany partnership was signed with the objective of bilateral cooperation for the development of the entire production chain of rare earth magnets. The project called *REGINA - Rare Earth Global Industry and New Applications*, involves several German and Brazilian institutions, and aims to develop magnet manufacturing technologies based on REEs.

Given the high added value of the raw material, the scarcity of resources and the environmental impact, it is important to investigate the process of machining these magnets not only by conventional manufacturing methods, for example cutting turning and grinding, but also with processes such as wire electrical discharge machining. It’s important to better understand how this thermal process will impact factors like surface damage and magnetic properties.

1.2 – OBJECTIVES

1.2.1 - Main objective and specific objectives

The main objective of this study is to evaluate the influence of wire electrical discharge machining parameters on the surface, roughness, subsurface and magnetic properties of machined Nd-Fe-B samples. In this context, the specific objectives are presented below:

- Investigate the surface generated by different cutting conditions through optical microscopy and scanning electron microscopy;
- Measure the roughness parameters Ra, Rt, Rz and Rq for the different cutting conditions and correlate results with characteristics of each condition;
- Make a general analysis of the surface and sub-surface using the pre-polishing methodology;
- Evaluate the magnetic potential impact on the hysteresis curves, remanence and coercivity of Nd-Fe-B samples machined via WEDM and correlate with microstructural changes.

2 – LITERATURE REVIEW

The fundamental concepts and theories of this work will be discussed in this section.

2.1 – ELECTRICAL DISCHARGE MACHINING

The wire electrical discharge machining process is a manufacturing process based on material removal using electrical discharges. Between the manufacturing processes, the norm DIN 8580 classifies EDM as being a “thermal removal” process, as illustrated in Figure 1.

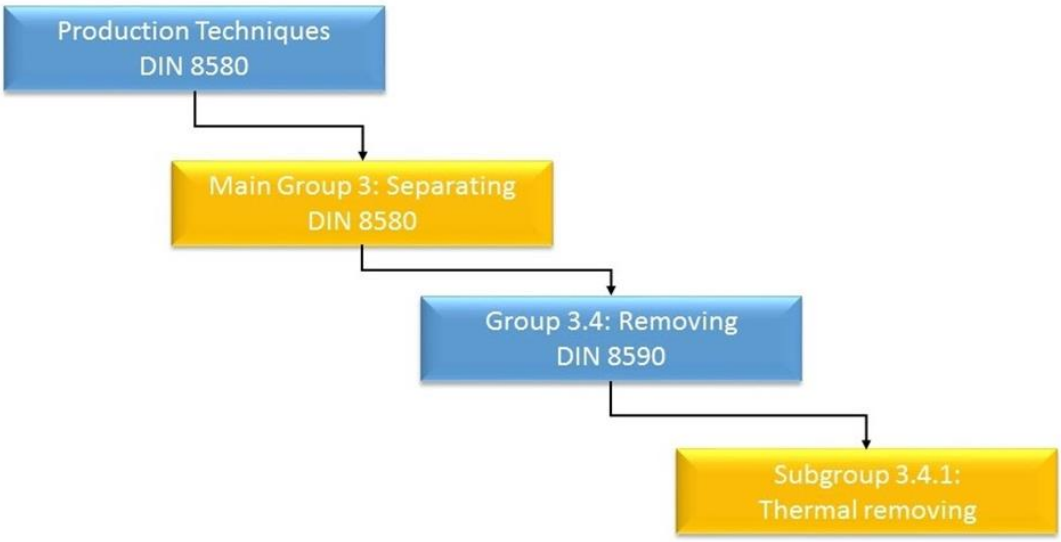

Figure 1 - Simplified DIN 8580.

2.1.1 - Electrical discharge machining removal phenomena

The physical, electrical, photonic and thermal phenomena that occur between a pair of electrically conductive electrodes immersed in a liquid or gaseous dielectric when submitted to a voltage are complex and not yet fully elucidated [6]. The most accepted model for an electrical discharge is explained in three steps, which are characterized by a combination of “skin” and “pinch”

effects. During the first step, there is an electrical potential difference gradient. The voltage between the electrodes accelerates the electrons, and in the path between the electrodes the electrons collide with the atoms and molecules of the dielectric, then transferring kinetic energy to the electrons of the atoms and molecules they collide with. This transfer of energy is manifested in three ways: vibrational, rotational energy of the molecules, and the lifting of electron orbits from the outer orbits of free atoms and atoms bound to molecules, causing an excitation and ionization by impact in the quantic level during the process, starting with the ignition (phase 1 from Figure 2) and ending when the voltage is turned off and the debris are expelled from the cutting zone (phase 4). If the collision energy is high enough, electrons from the last layers are thrown out of the domain of the atoms of the dielectric. Part of the energy supplied to the electrons of atoms and molecules that had previously collided with electrons is returned in the form of photons, making the phenomenon visible [6]. This mechanism and the fact that the electrodes are at a minimum distance for the discharge to occur ends up causing the dielectric to break and then an electrical discharge begins. Due to the skin effect, the current is restricted almost exclusively to the cylindrical surface of the newly formed discharge channel.

In the second stage of the discharge, the constant current is concentrated in a minimum section, due to the pinch effect. This current concentrated in the central region gives rise to the plasma channel, which has high temperatures in the order of 25.000 K. This extremely high temperature causes the fusion and evaporation of a certain volume of material, so that the plasma channel and the bubble gasses constantly increase. During the third stage, which starts with the turn-off of the electricity, the skin effect takes place one more time. After that, the gas bubble and the plasma channel collapse and the partially liquid and partially evaporated material is catapulted out, which is then the fourth step at the end of an electrical discharge cycle [7]. Figure 2 shows the stages of electrical discharge as well as the behavior of voltage and current during the stages.

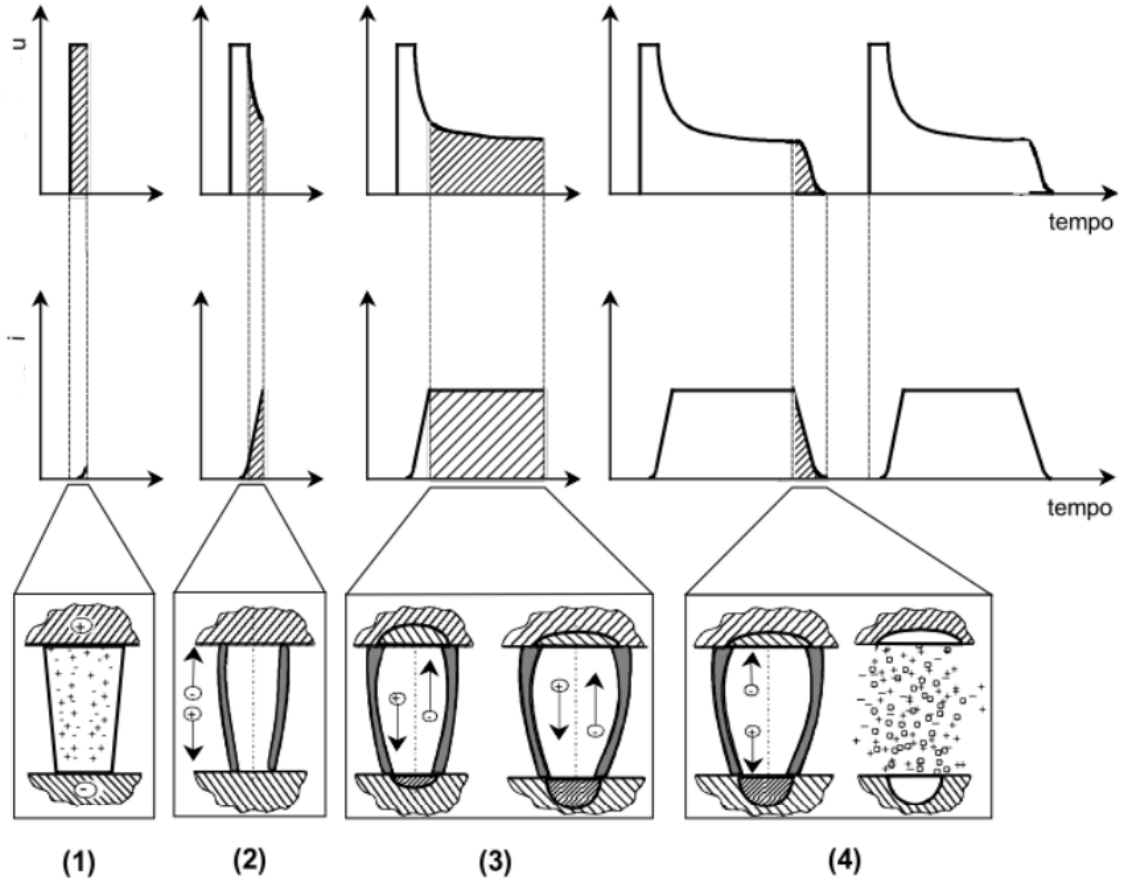

Figure 2 - Stages 1, 2, 3 and 4 of an electrical discharge [7].

2.1.2 - Parameters during an electrical discharge machining process

The process explained in the previous sub-section can be examined with more details on the graphics of current and voltage per time. As it can be seen, the voltage increases and a discharge between the electrodes happens, repeating this cycle during the material removal. The initial phase, termed the ignition phase, signifies the duration during which the high open circuit voltage $\hat{u}_i$, applied across the working gap, transitions to the relatively lower discharge voltage ue, typically ranging between 10 and 40 V. This time interval is referred to as the ignition delay time, denoted as t_d [μ_s]. Following this, the second phase commences immediately, characterized by a rapid surge in current to the discharge current $\hat{i}_e$ [A], resulting in the formation of a plasma channel enveloped by a vapor bubble.

The third phase, known as the discharge phase, involves the sustained presence of a high-energy, high-pressure plasma channel for a specified duration, represented as t_e [μ_s]. This phase leads to the melting and evaporation of a small amount of material from both the electrode and the workpiece.

The fourth and final phase, marking the conclusion of the process, is the collapse of the plasma channel when the electric energy is deactivated, leading to the forceful ejection of molten material. This moment, termed the interval time (t_o [μ_s]), involves the expulsion of a portion of the molten and vaporized material due to the flow of dielectric fluid across the gap, while the remainder solidifies in the newly formed crater and its vicinity.

Throughout the interval time (t_o), there is also a cooling process for the electrode and workpiece, accompanied by the de-ionization of the working gap. These steps are crucial to facilitate the effective dispersion of subsequent discharges across the surfaces of both the electrode and the workpiece. This iterative process continues until the desired part geometry is achieved [8]. The parameters explained above are shown in Figure 3, which the first graphic shows the voltage per time in milliseconds and the second graphic the maximum current during discharge per milliseconds.

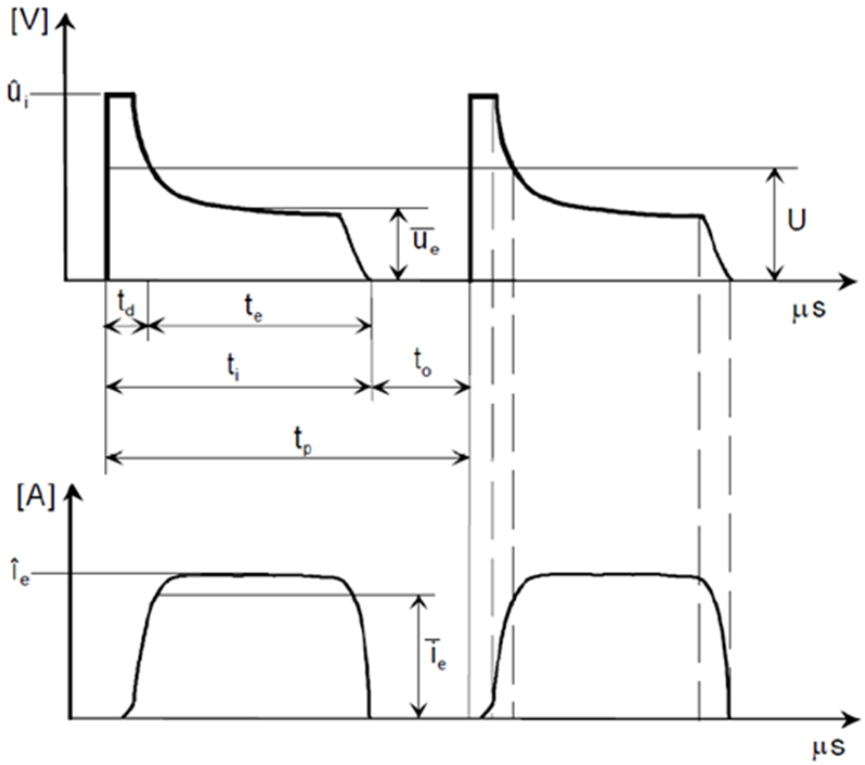

Figure 3 - Discharge diagram for EDM [9].

- ûi [V] – Voltage between part and electrode before the discharge;
- ûe [V] – Average voltage while discharge occurs;
- U [V] – Average voltage during the whole machining operation;
- td [µs] – Delay ignition time, which is the time interval between application of voltage ûi and beginning of discharge;
- te [µs] – Discharge duration time, which is characterized by the time when the dielectric tension is broken and the discharge is occurring;
- ti [µs] – Pulse on time, which represents the pulse duration time td + te;
- to [µs] – Pulse off time, which represents the time between two consecutives discharging time on ti;
- tp [µs] – Discharge cycle time, represents the sum of ti + to;
- îe [A] – Maximum current during discharge;
- Īe [A] – Average current during discharge;
- τ - Duty factor, represents the ratio between time on (ti) and discharge cycle time (tp);

Since this is a thermal process, all the parameters that influence the amount of energy delivered to the cutting zone like intensity of the current, for example, will generate a damaged surface due to the thermal impact generated by the discharge. As observed by another authors, an increase in the discharge current will have an effect on surface integrity, the increase of the pulse time will also affect the level of damage proportioned to the material being machined. For machining conditions with high energetic input in the parts, the remained surface is likely to have a poor-quality result. Non-uniformity of recast layer, incidence of multiple pores, and cracks characterize those surfaces machined with more aggressive machining conditions. [9]

2.1.3 - Variations of electrical discharge machining process

One of the advantages of the EDM process is its high application flexibility in relation to the electrode geometry. In the case of EDM by penetration it is possible to make engravings, cuts with samples and holes. It is also possible to perform cutting with disk, wire, flat and planetary grinding [10]. Figure 4 illustrates some forms of application for the EDM process.

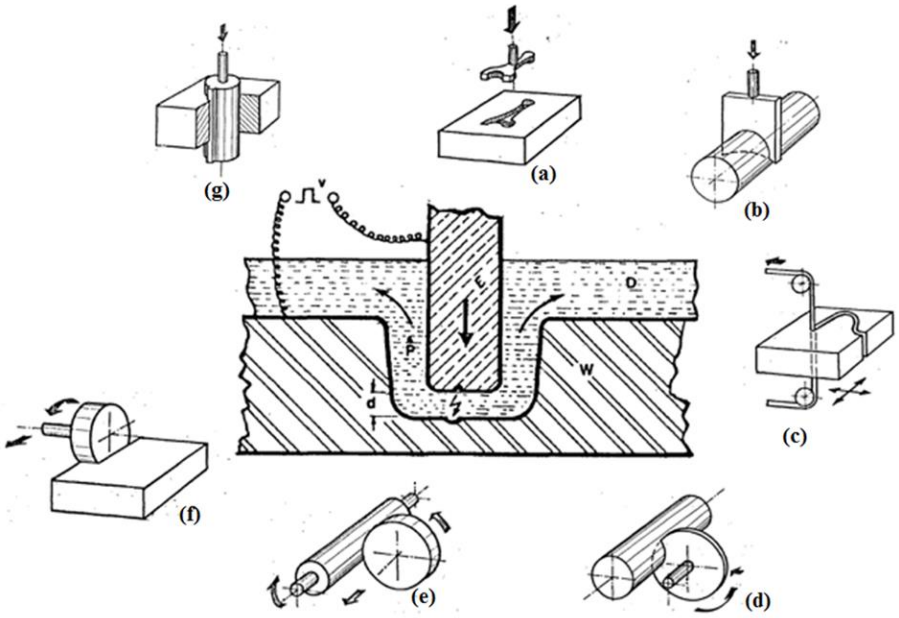

Figure 4 - Electrical discharge machining by (a) diving, (b) blade, (c) wire, (d) disk, (e) planetary gringind, (f) plane gringing and (g) drilling [10].

In the case of penetration EDM, the tool electrode will have the negative shape of the part and can be made of metallic material or other materials such as graphite for example.

2.1.4 - Wire electrical discharge machine basic scheme

In the case of wire EDM, the electrode will necessarily be a metallic wire composed usually of molybdenum or tungsten with diameter usually ranging from 0.05 to 3.00 mm. In addition, the part in an WEDM process can be submerged in the dielectric fluid or can be subject to a jet of dielectric fluid, so that the dielectric fluid is directed to the working gap (contact region between electrode-tool and electrode-piece), as illustrated in Figure 5. With respect to the wire, it may or may not be continually renewed and its movement may be continuous or reciprocating.

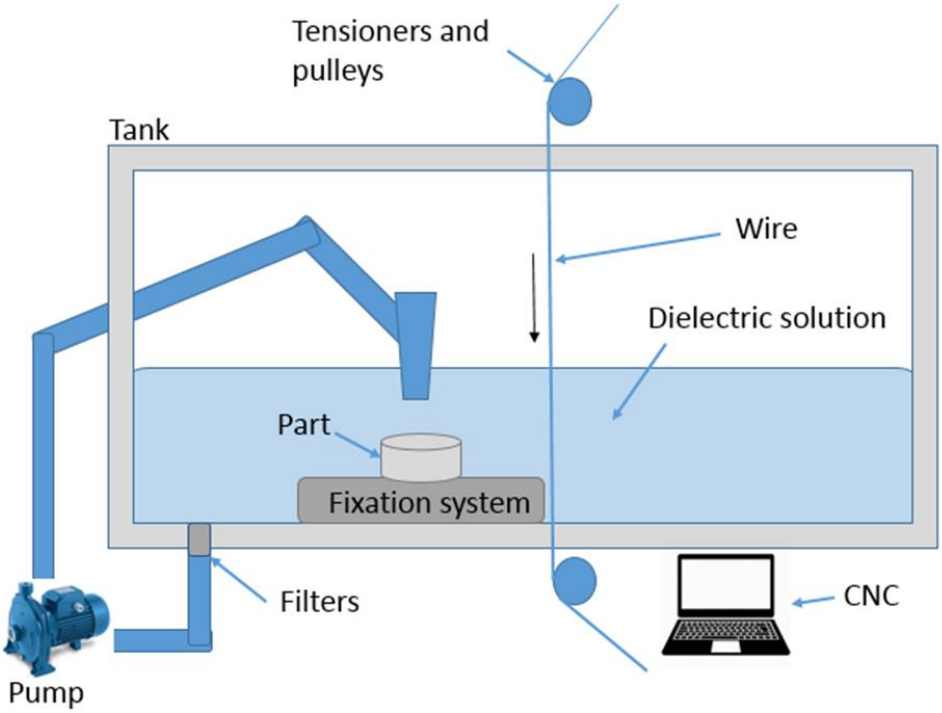

Figure 5 - Wire electrical discharge machine basic scheme.

The tensioning of the wire is done by means of pulleys that also serve to position the same. Wire control is carried out by computer numerical control, which programs the path of the wire. The fixation system is often composed of bars, screws and staples to fix the part. Since EDM is a process that doesn't

involve forces, the part fixation could even be done with magnets. Another peculiarity of wire EDM is the fact that the dielectric used is generally demineralized water. Regarding dielectrics based on hydrocarbons, demineralized water has good washing conditions and there is no formation of solid products resulting from the decomposition of the dielectric [8].

The EDM process has many advantages over conventional machining processes. Among them we can mention the ability to generate highly complex geometries, the ability to machine materials with high hardness and great flexibility of the process. As a disadvantage, it can be mentioned that only conductive materials can be machined by EDM, the high heat input due to electrical discharges and the complexity of the process in regarding the phenomena during the discharge [10, 11].

2.2 – NEODYMIUM-IRON-BORON MAGNETS

The maximum energy product $(BH)_{max}$ is a measure of the magnetic energy density that can be stored in a magnetic material. The maximum energy product $(BH)_{Max}$, which is the main indicator of the strength of a magnet, provides a figure of merit with respect to the magnetic performance of magnets. Sintered Nd-Fe-B magnets have received a lot of attention since their development in the early 1980s [12]. The graph in Figure 6 illustrates the evolution of the $(BH)_{Max}$ of several magnets over the last 100 years, where the cylinders give and idea of (BH)max per volume for the different magnets. Noting that rare-earth based magnets have a considerably higher maximum energy product than those that do not have these elements, with an emphasis on the Nd-Fe-B magnets [13].

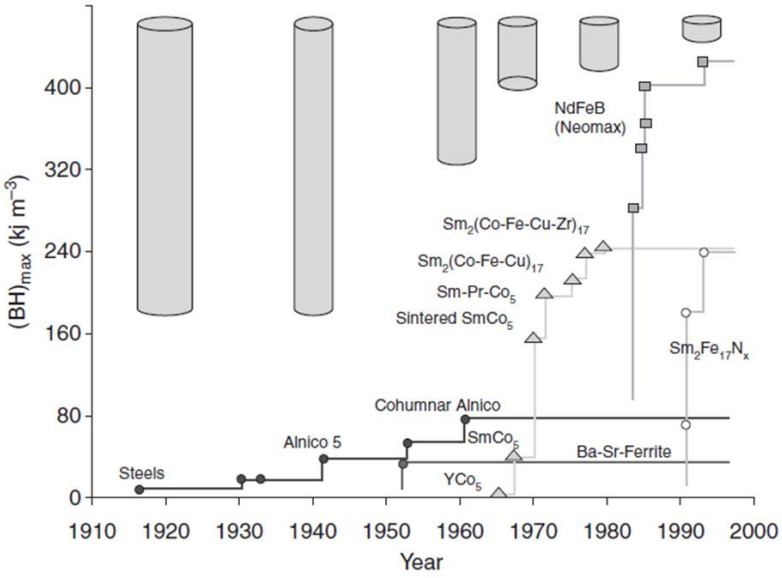

Figure 6 - The evolution of the (BH)Max over 100 years [13].

2.2.1 – Structural properties of Nd-Fe-B magnets

Intermetallic compounds of certain rare earths and transition metals can be transformed into permanent magnets with high remanence and coercivity through processing via powder metallurgy. In this process, the compounds are reduced into particles of size in the range of a few micrometers, and then compacted and aligned under the application of an external magnetic field. By this process the magnet becomes anisotropic and has its energy-product maximized in one specific direction. The mechanical strength of the compact, as well as the alignment of the particles, is a consolidated treatment

The Nd-Fe-B magnets are constituted by a primary $Nd_2Fe_{14}B$ whose crystal structure is tetragonal, containing 68 atoms per cell unit [13], as illustrated in Figure 7. The primary phase has received great importance due to its excellent intrinsic magnetic properties. However, it is known that the magnetic properties of Nd-Fe-B magnets strongly depend on the microstructure, distribution, composition and properties of the neodymium-rich phase [14].

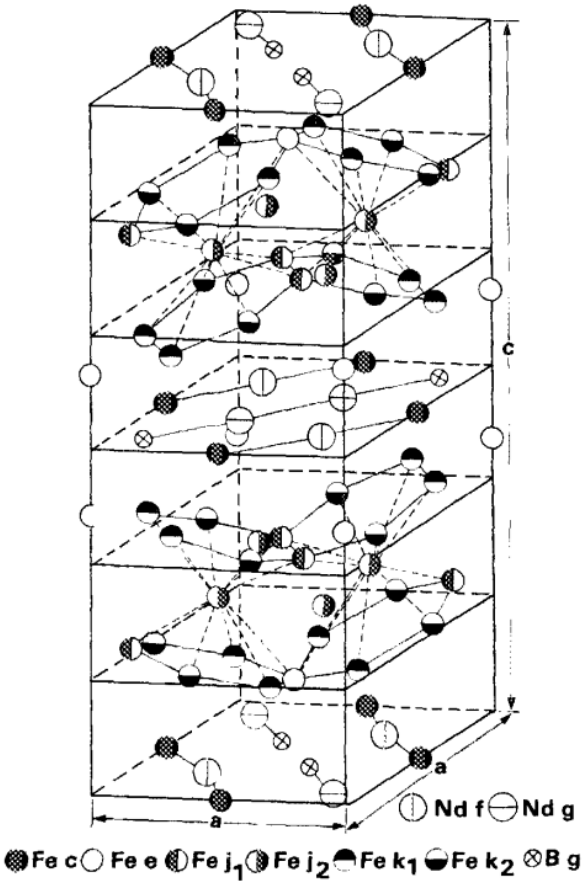

Figure 7 - Tetragonal unit cell of Nd based rare-earth magnets [13].

During the sintering process another phase rich in Nd is formed with the presence of a liquid phase. Several researches have shown that this rich phase is found in grain boundaries and in triple points, observed as thin layers in the nanometric order [13, 14], as illustrated in Figure 8.

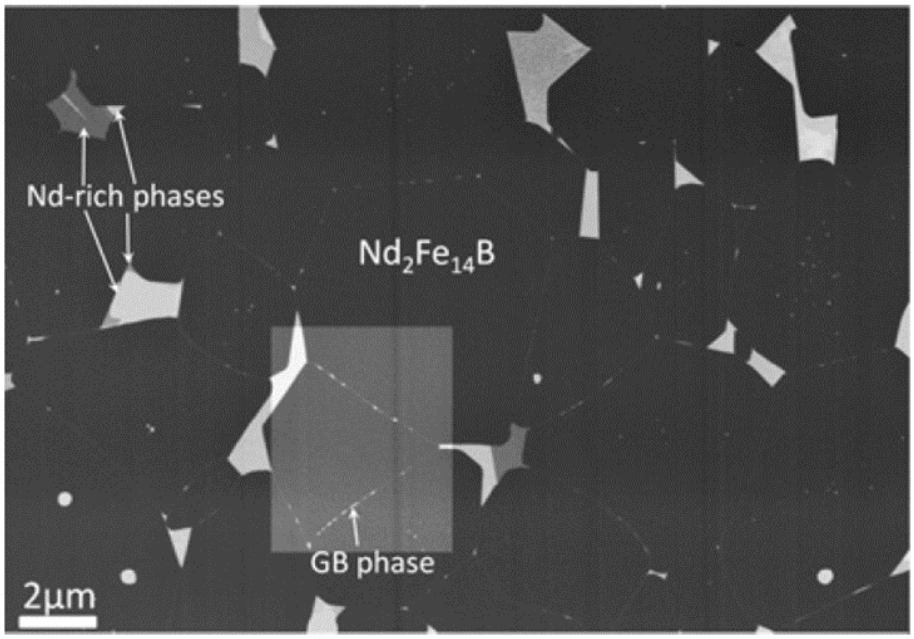

Figure 8 - Typical high-resolution backscattered electron (BSE) scanning electron microscopy (SEM) image of a sintered Nd-Fe-B permanent magnet [13].

In Figure 8, the dark gray regions correspond to the crystal grains of the $Nd_2Fe_{14}B$ phase. Brightly imaging areas are so-called “Nd-rich” areas, which are mainly present at triple junctions of grain boundaries. There are at least two contrasts in the Nd-rich phase triple junction grains, suggesting the existence of multiple phases. Grain boundaries are also observed with inhomogeneous contrast [14].

2.2.2 - Nd-Fe-B magnets manufacturing

The production of Nd-Fe-B magnets involves several steps. After being reduced to metallic form with an ingot format, they are submitted to the casting process in vacuum induction furnaces [15]. The molten alloy can be cooled and deposited in molds for the production of ingots or rapidly cooled in the form of ribbons by the “strip-casting” process, which consists of the fast solidification of the metal when it comes into contact with a cooled disk [16].

Once the alloy has solidified, the hydrogen decrepitation technique is used to break up and brittle the material as shown in Figure 9. The use of hydrogen in the manufacture of rare earth magnets has been studied since 1978 and in the case of Nd-Fe-B magnets the interaction between the hydrogen atoms with the alloy leads to an exothermic reaction, which in turn leads to a decrepitation of the

ingot [16]. After decrepitation, the material is submitted to the milling process to reduce the particle size, in order to achieve a particle size between 3 μm and 15 μm [15, 16].

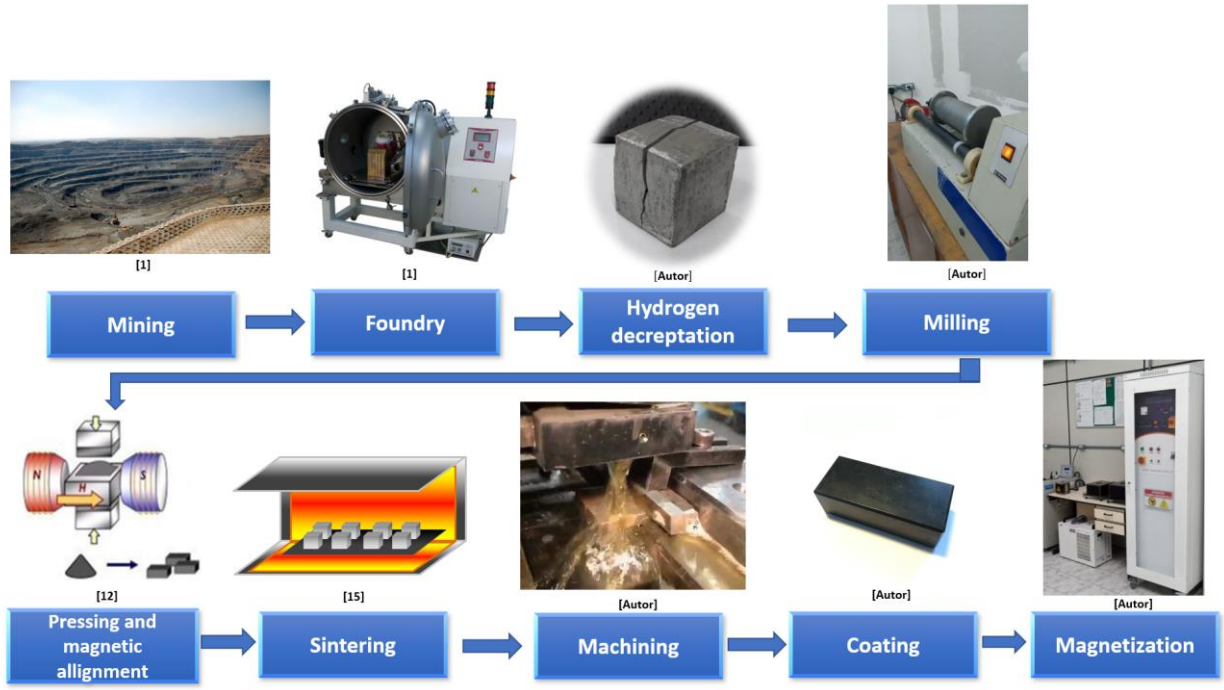

Figure 9 - Simplified manufacturing process of Nd-based rare-earth magnets.

These particles can be compacted and aligned under the presence of a magnetic field or not. It is noteworthy that the non-application of a magnetic field during compaction generates a non-textured or isotropic magnet [15]. After compacting, the magnets are subjected to a sintering heat treatment, with temperatures in the range of 1000 - 1100 °C under high vacuum, or under an inverted atmosphere to reach more than 95% of the theoretical density. Once sintered, the magnets are machined. After the machining, the magnets must be coated, as they are highly reactive in the presence of oxygen. Coatings can be in the form of monolayers with materials such as nickel, copper, chromium, zinc, epoxy, gold or multilayer [17]. Once coated, the magnets are magnetized and ready to use. Figure 9 illustrates the whole basic process of manufacturing sintered Nd-Fe-B magnets. Nd-Fe-B magnets have been used in many engineering applications, being part of the magnets developed for engines, as long as other magnetic compounds [18].

2.3 – ELECTRICAL DISCHARGE MACHINING OF Nd-Fe-B MAGNETS

Nd-Fe-B magnets emerged as an economic alternative, despite the complexity of its manufacturing. Another factor that adds to the complexity of manufacturing Nd-Fe-B magnets is the fact that these magnets are known to be fragile materials with high hardness, low machinability, which requires the search for more appropriate machining techniques for these materials [19].

In the EDM of Nd-Fe-B magnets, a good surface quality can be obtained using low current discharges and short pulse duration. As the pulse duration increases, the singular energy of each discharge increases and causes greater and deeper damage to the surface, thus decreasing the re-solidification of the molten material [20, 21]. The current also influences the surface quality of magnets machined by EDM. As illustrated in Figures 10 and 11, using a current above 27 A, the microcrack formation mechanism is intensified and there is a rapid deterioration in surface quality [22, 23].

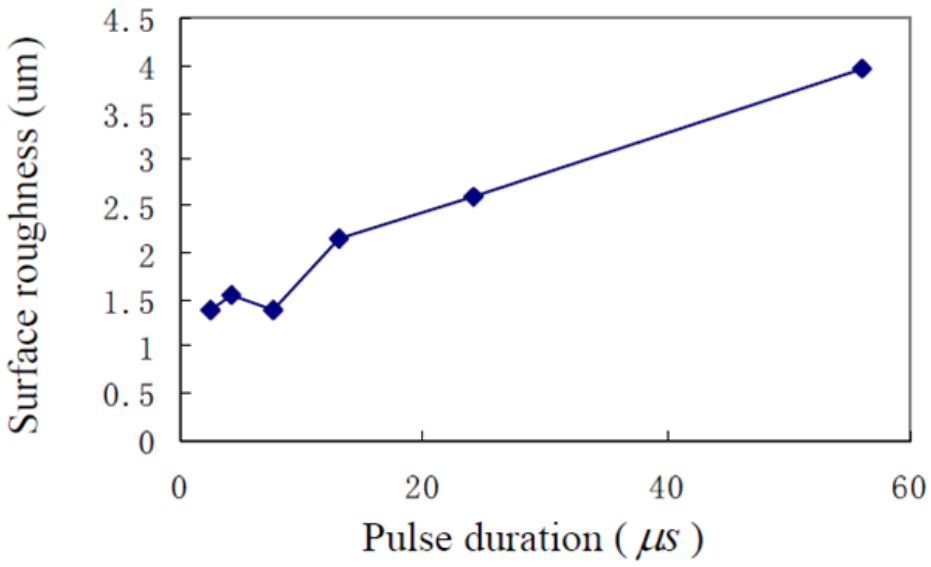

Figure 10 - Relationship between pulse duration and surface roughness (peak current: 14.2 A; pulse off time: 18 μs) [23].

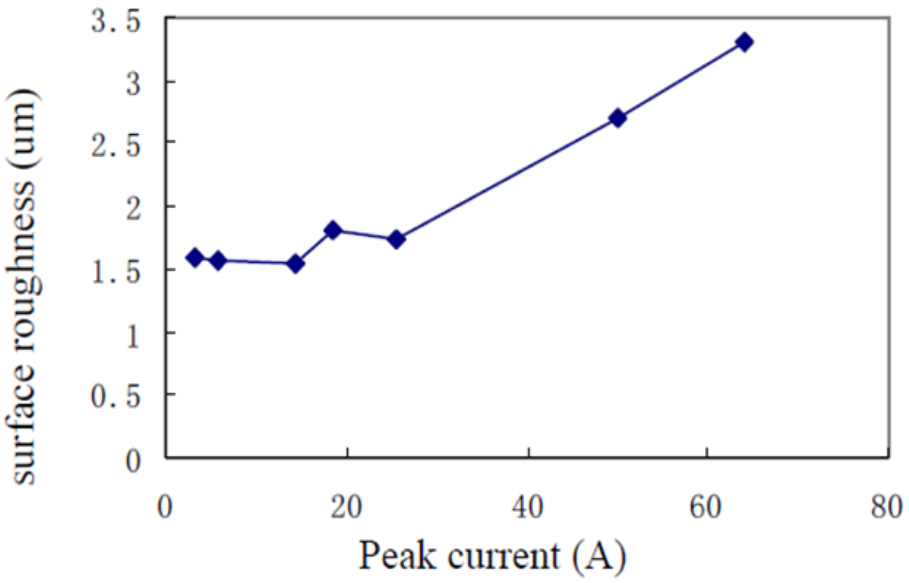

Figure 11 - Relationship between peak current and surface roughness [23].

Being a fragile material, Nd-Fe-B magnets have little resistance to tensile stresses [23]. When subjected to EDM, the surface of these magnets undergoes a large and instantaneous temperature variation, which results in the formation and propagation of thermal cracks. When the material is subjected to this thermal cycle, a complete temperature gradient is established based on the properties and flux of the dielectric as well as the properties of the materials. With the sudden heating, local shear stresses arise because the material that is expanding cannot be separated from the material that is in the interior and with a lower temperature. The situation is reversed in sudden cooling and when these internal stresses are greater than the binding strength of the material, breakage or removal of whole grains occurs [22].

The machining of Nd-Fe-B with electrical discharge machining can leave different surface defects such craters and presence of cracks. When these cracks connect, they can cause the removal of a whole grain [22]. Figure 12 illustrates the chips derived from the EDM of Nd-Fe-B magnets, the thermal cracks formed and the grain removal mechanism.

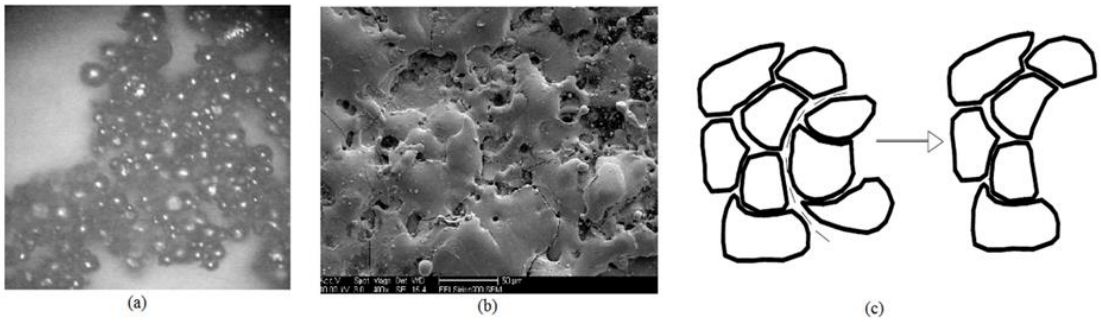

Figure 12 - (a) Picture of debris, (b) microstructure of machined surface and (c) model for whole grain removal [23].

2.4 – VSM AND MAGNETIC PROPERTIES

The Vibrating Sample Magnetometer (VSM) is based on the vibration of a sample in a magnetic field to produce an alternating electromotive force (EMF) within a set of suitably placed pick-up or sensing coils. This induced EMF is directly proportional to the magnetic moment (m) or magnetization (M) of the sample under test. VSM's are used widely, since magnetic properties can be measured for a diverse range of sample sizes and configurations, i.e., powders, solids, single crystals, thin films, and liquids, and because they are particularly well suited to allow measurements at both low and high temperatures. In the development of rare-earth magnet materials, the VSM has been used extensively to measure saturation, remanence, coercivity, anisotropy fields, etc., and also to measure temperature dependent parameters of interest, for example Curie temperatures. The VSM is an open loop measurement in that the sample and field source (e.g., electromagnet) do not constitute a closed flux line loop. Hence, the measured parameters must be corrected for demagnetization effects to yield the true intrinsic material parameters most often of interest for permanent magnet materials. In the open loop measurement, the internal field experienced by a sample differs from the applied field owing to an internal demagnetizing field which depends on the sample geometry under test [25].

The VSM measures magnetic moment (m) as a function of applied field $H_{Applied}$. The equations that relate open loop (VSM) to closed loop measurements are:

8

$$M = m/V$$

Where Magnetization “M” has (A/m) unit, “m” is the moment measured by the VSM and given in electromagnetic unit (emu) and V is the sample volume in cubic centimeters.

The internal magnetic field H is given in (kA/m) and it’s related to the applied field H_A also given in (kA/m) by the following equation:

$$H = H_{Applied} - N_d M$$

Where N_d = sample demagnetization factor. Values for N_d may be determined empirically or analytically, with these equations is possible to treat the data obtained with VSM and to plot the hysteresis curves for all samples machined with different conditions.

The magnetic induction B (T) is given by the following equation:

$$B = \mu_o (H + M)$$

Where μ_o is the vacuum magnetic permeability and equals to $4\pi 10^{-7}$ $T.m.A^{-1}$. With this equation is possible to obtain the hysteresis curves of magnetic induction as a function of the internal magnetic field and magnetization.

A ferromagnetic material, when in the presence of an external field (H) can be represented by a magnetic induction (B) as a function of this external field in a graphic called hysteresis curve [26, 27]. Figure 13 represents a hysteresis curve for a ferromagnetic material.

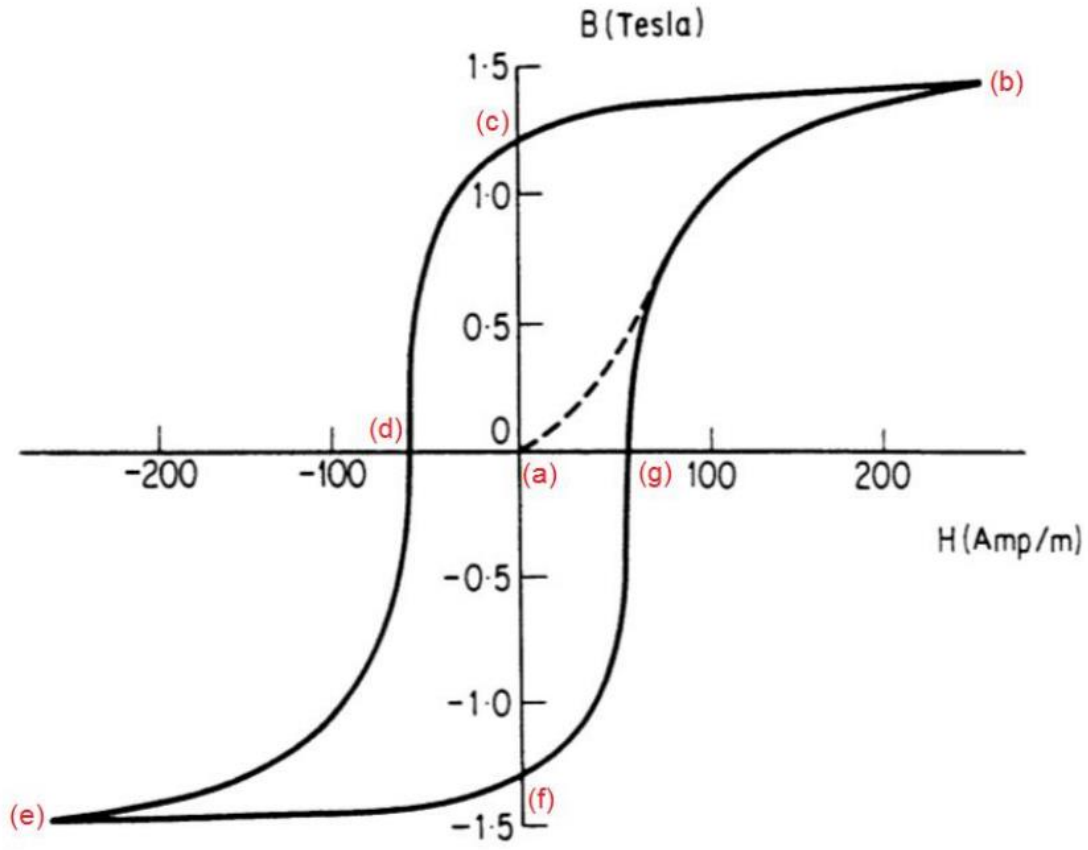

Figure 13 - Typical hysteresis cycle of a ferromagnetic material [27].

In the first quadrant of the hysteresis cycle it is possible to observe a dashed curve that represents the magnetization process. Point (a) indicates that H = 0 and that the material has misaligned magnetic domains. By increasing the intensity of the applied field, point (b) is reached, which represents the saturation magnetization (M_s). Point (c) is reached by ceasing the application of external field, which represents the remaining magnetic field in the material, a property known as remanence (B_r) [28, 29].

If a field with the same intensity is applied, but with opposite polarity, called the reverse field or demagnetizing field (-H), the point (d) is reached in the second quadrant of the hysteresis loop. This point indicates the field required to reduce the magnetic induction to zero, and is known as coercivity ($_iH_C$). When the application of the reverse field persists, point (e) is reached, which is the saturation magnetization, but with the opposite polarity to that observed in point

(a). Analogously, the whole process is repeated in (f) and (g), and the complete hysteresis loop is formed [30, 31]. The concepts reviewed in this chapter will help to understand the planning of this work, as well as the results which will be presented in chapter 4.

3 – MATERIALS AND METHODS

This section will present the materials and methods used for the development of this work.

3.1 – ACTIVITIES FLOWCHART

The first step of this work was to machine samples from a wind-turbine block. This block was machined down to samples having 5 mm by 5 mm of area and height equals to 250 µm. The samples were machined by the machine that will be presented in section 3.4 and then the samples were submitted to a roughness, general surface morphology and magnetic properties analysis with the equipment presented in this chapter. Figure 14 shows the activities flowchart for the Part I of this experimental work, which aimed obtaining results of roughness, general surface and magnetic properties.

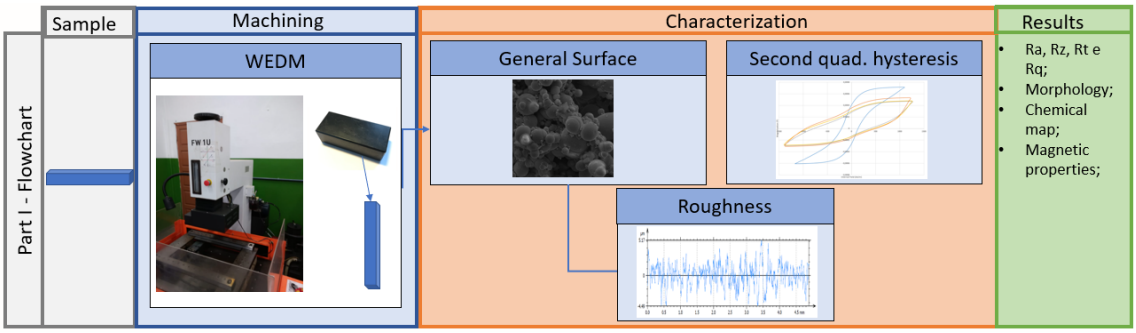

Figure 14 - Activities flowchart - Part I.

The Part II of this work was planned to study how the machining process would affect the cross-sectional layer of the samples. In order to do that, the samples were prepared using a pre-polishing methodology as shown in Figure 15.

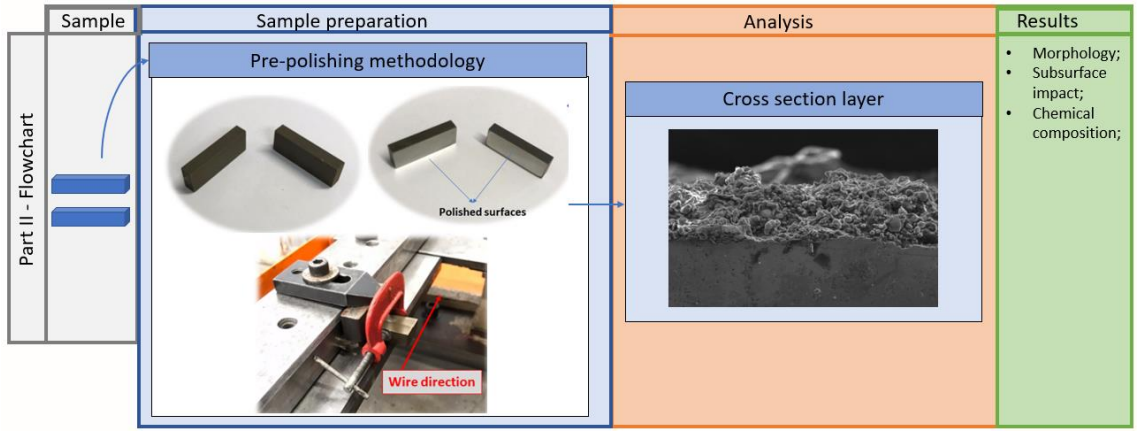

Figure 15 - Activities Flowchart - Part II.

This methodology consists of preparing two samples that would be at first polished and then positioned face to face, after they were positioned in the machined the machining process was done transversally to the height of the samples in order to study how much the cut would affect the sub-surface of the samples. Figure 18 shows the second part of this work which aimed to study the cross-sectional impact on the samples after machining.

3.2 – CHARACTERIZATION EQUIPMENTS AND LABORATORIES

In this section the experimental equipment used in this work will be discussed. The evaluation of the experiments was made with the support of the staff and equipment of several partners:

- LMP - Mechanical Precision Laboratory;
- MAGMA - Magnetic Material Group;
- IFSC - Federal Institute of Santa Catarina;
- LCM - Laboratory for Microstructure Characterization;
- LABMAT - Materials Laboratory;

- LabCAM - Multiusuary Laboratory for Magnetic Materials Characterization;
- CERMAT - Ceramic and Composite Materials Research Center.

3.3 - Nd-Fe-B SAMPLE

The first part of the experimental procedure used in this work was to machine Nd-Fe-B samples from a commercially available Nd-Fe-B grade N42 coated block used in wind turbines. The wind turbine magnet had two different coatings. The two coatings were removed with acetone (CH_3COCH_3) prior to the machining process. The wind turbine block dimensions were a transversal section of 29 mm per 38 mm and 91 mm length shown in Figure 16. The block was then machined down to a workpiece with 5 x 5 mm² section and 29 mm length, the direction of the workpiece length is the easy magnetization (Z axis).

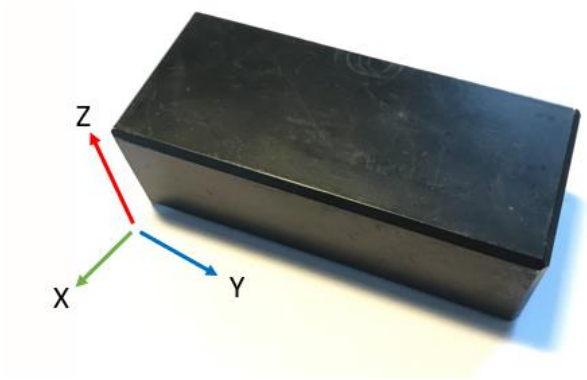

Figure 16 - Half of the initial magnet block and its layers along with workpiece and microblade samples.

The workpiece was fixed in the machine with staples and machined in samples with a blade shape transversally to the easy magnetization direction according to Figure 17, the samples needed to be machined like this in order to make it possible to observe their magnetic properties with VSM analysis. The samples once machined were cleaned with acetone and stored in an anaerobic chamber.

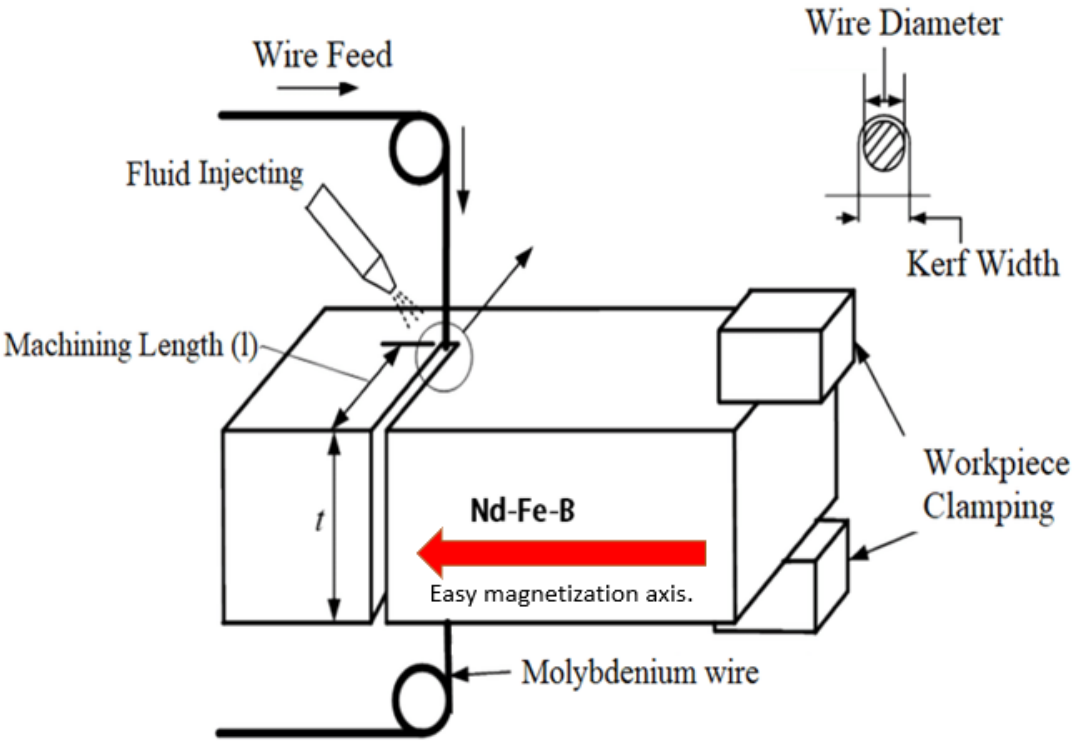

Figure 17 - Fixed sample [31].

3.4 - AgieCut CHALLENGE FW1U MACHINE

The machine used to carry out the experimental cuts is a wire EDM machine model AgieCut Challenge FW1U from the Swiss machine manufacturer Charmilles. Figure 18 shows the machine available at IFSC. The machine is controlled by computational numerical control (CNC) and can exchange data with other computers and control systems. The movement of the fixing table in X, Y, U and V can be carried out roughly by manual control coupled to the machine or precisely by supplying the desired position.

Figure 18 - AgieCut Challenge FW1U available at IFSC.

3.5 – MOLYBDENIUM WIRE

The tool chosen for the experiments is a commercially available molybdenum wire with 0.18 mm diameter. This tool is recommended by the manufacturer's manual and is known for being flexible which avoids the breakage of the wire during the machining process.

The workpiece was fixed in the machine with clamps, performing the machining of the samples. The wire direction is perpendicular to the easy magnetization direction. It's important to note that the workpiece samples were not magnetized.

3.6 – MACHINING CONDITIONS

The machining conditions were chosen among the available options in the machine and based on literature and the equipment manual [33, 34, 35]. Table 01 was taken from the manufacturer's manual and shows 4 standard machining

conditions that were used in this experimental procedure. The condition C821 is classified as a roughing condition, which has a higher energy input and in turn causes more damage to the surfaces. Condition C822 can be classified as semi-finishing, and conditions C823 and C824 are classified as finishing conditions, which have less energy input and therefore they do not damage the machined surface as much as the roughing conditions [35, 36].

Table 1 - Main eroding parameters in FW1U WEDM machine.

Machining condition	Cond No,	ON (µs)	OFF (µs)	IP (A)
Roughing	C821	24	15	7.0
Semi-finishing	C822	05	04	3.0
Finishing	C823	31	31	2.0
Finishing II	C824	31	01	2.5

Table 2 - WEDM machine parameters.

ON	Pulse duration.
OFF	Time between two pulses.
IP	Peak current.

3.7 - RUGOSIMETER

A Taylor Hobson profilometer model Form Talysurf il20 [37] (Figure 19a) with a 2 μm stylus tip radius was used to perform the roughness measurements. The measurement speed was set to 2 mm/s and a 2CR PC filter where the first and the last sample length was used. According to the norm ISO 3274 [38], it's necessary a 5.6 mm length in order to measure roughness. However, three cut offs of 0.8 mm were measured in order to perform the roughness analysis. The equipment has a 0.001 μm systematic error guaranteed by the manufacturer [39].

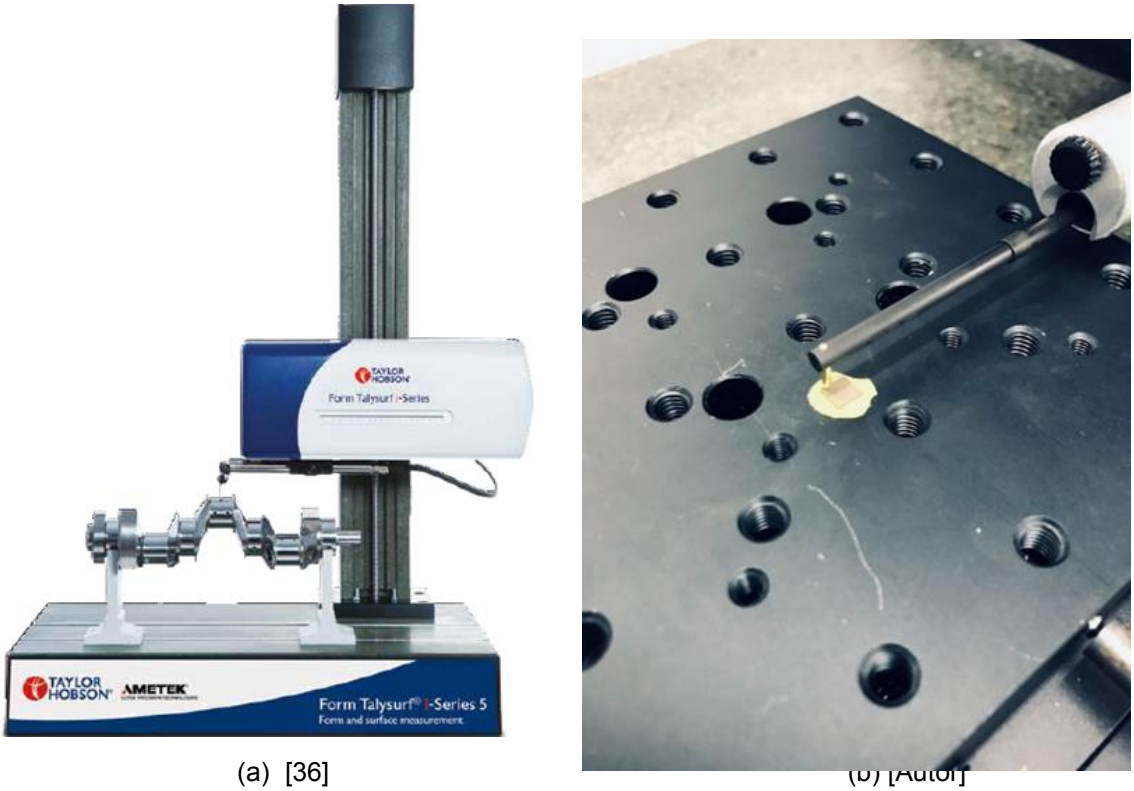

(a) [36] (b) [Autor]

Figure 19 - (a) Taylor Surf il20 rugosimeter and (b) Measurement of Nd-Fe-B sample fixed with plasticine.

For the roughness analysis, a total of 60 samples were machined, 15 samples for each machining condition. The samples were aleatory analyzed with

the rugosimeter in order to obtain the roughness parameters generated by each machining condition. The samples were fixed with plasticine and then measured as shown in Figure 19b. The experiments were repeated twice for each blade summing up a number of 120 experimental results. These results were treated with Digital Surf Software.

3.8 – SCANNING ELECTRON MICROSCOPES

Two scanning electron microscopes were used in order to evaluate surface integrity. The first microscope is from the manufacturer HITACHI model TM3030Plus. It was used to analyze samples with a maximum ampliation of 2000 times. For further ampliations another microscope was used, this one had the capability of 10000 magnification and it's a Vega3 Tescan scanning electron microscope. Both microscopes were used with a voltage of 20kV and using the imaging functions of secondary electrons (SE) and back-scattered electrons (BSE) for chemical compositional information. Figures 20 and 21 present respectively the microscopes TM3030Plus available at CERMAT and VEGA3 Tescan available at LabMat.

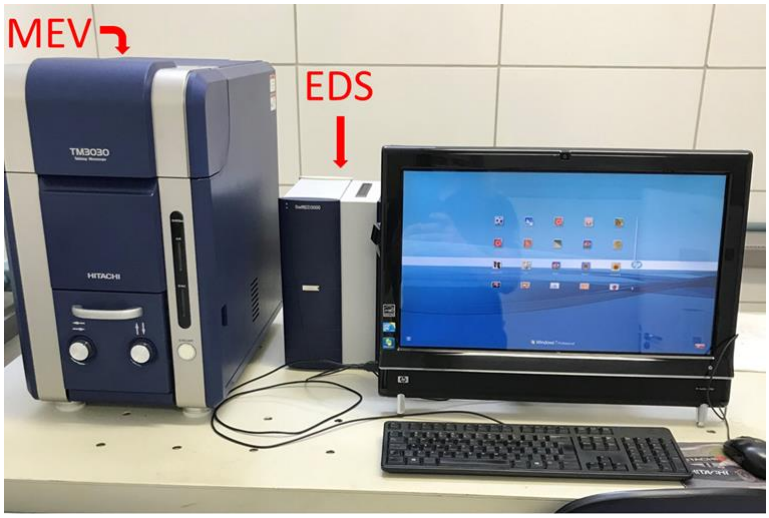

Figure 20 - TM3030 Plus from CERMAT.

Figure 21 - VEGA3 Tescan SEM available at LCM.

The specimens were attached in the metallic support with double face tape for the surface analysis as shown in Figure 22. For the affected layer analysis, the pre-polishing methodology described in the beginning of this section was used.

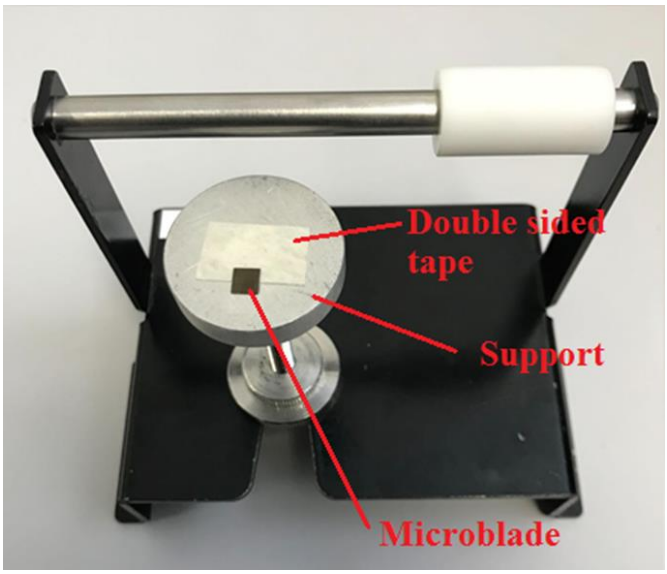

Figure 22 - Nd-Fe-B sample attached to support for surface evaluation.

3.9 - PRE-POLISHIMG METHODOLOGY

An analysis of the cross section was performed in order to investigate the depth of the damage suffered by the material when machined by the C821 machining condition and the finishing condition C824. Blocks were prepared with the pre-polishing methodology. This methodology consists of polishing two blocks with several sandpapers. After they are polished, the two surfaces are placed together and the cut is made in the transversal direction to the polished surfaces, as showed in Figure 23. The sandpapers used were with 80, 120, 220, 400, 600, 800, 1200, 1500, 2000, 2500, 3000 and 4000 grain size. The cross-sectional results were obtained with a Vega3 TESCAN scanning electron microscope, it was possible to observe the border's morphology and spectrums.

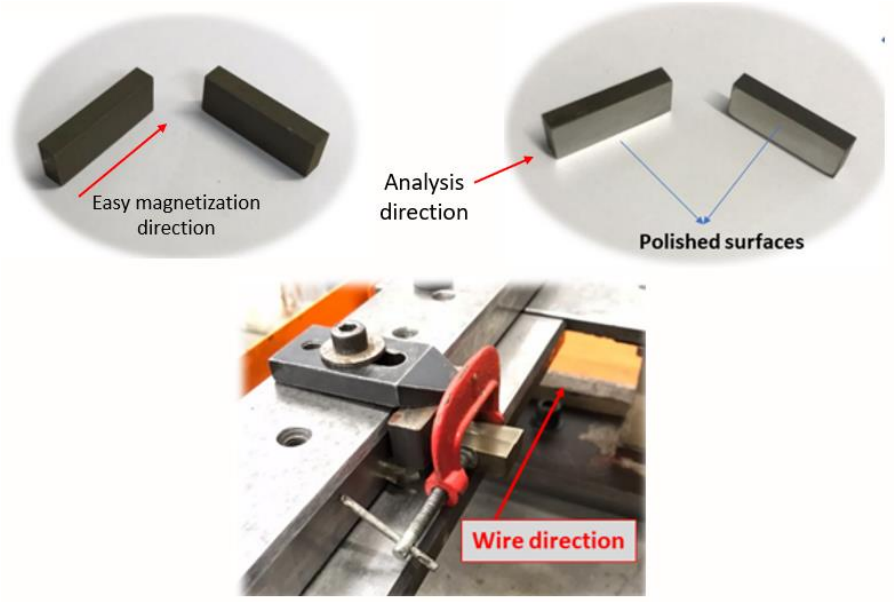

Figure 23 - Pre-polishing methodology.

3.10- EV9 VSM

The EV9 vibrating sample magnetometer (Figure 24) can reach fields up to 26 kOe at a sample space of 5 mm and 21.5 kOe with the temperature chamber in place.

Figure 24 - EV9 Vibrating sample magnetometer [40].

The samples were attached to the rod support with white grease and covered with non-magnetic Teflon tape to avoid sample displacement. The direction of easy magnetization is on the thickness direction of the samples as shown in Figure 25.

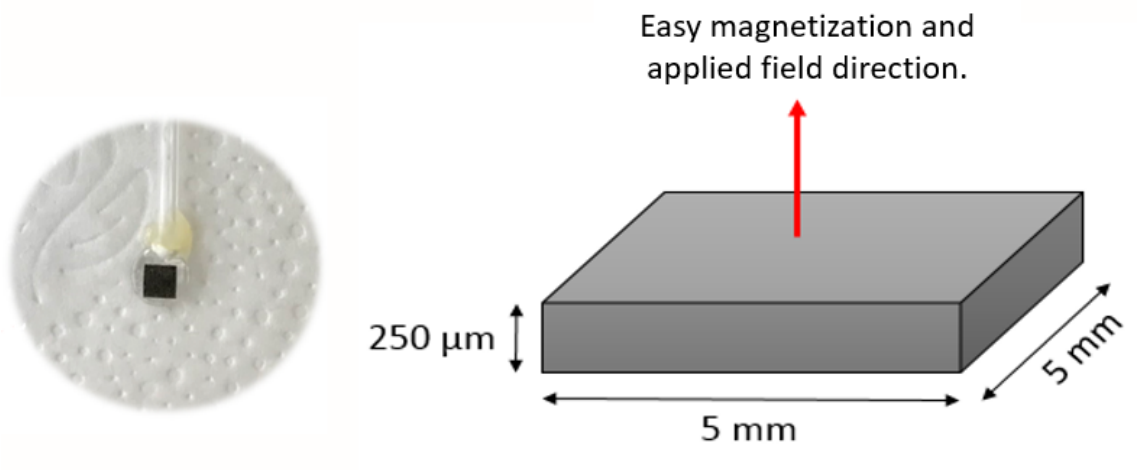

Figure 25 - Sample preparation for VSM analysis.

The sample used in this experiment has 5 mm sides and 250 µm height as shown in Figure 25 and its volume is equals to 0.00625 cm³. For the sample in question, taking in consideration it's dimensions and shape and according to the litterature, the demagnetization factor (Nd) is equals to 0.875 [40, 41]. The magnet samples were magnetized with 4.5 T with a magnetic pulse and afterwards analyzed in the VSM. The selected field setup started in zero field and went down to - 20 kOe with a 800 Oe step. This setup was design to obtain remanence and coercivity as well as second quadrant of hysteresis curve. Due to machine availability, an in order to optimize experiments, it was decided that only the roughing and the second finishing condition would be examined with VSM analysis.

4 - RESULTS

The results will be presented by type. First the roughness results will be presented along with optical microscope results, followed by surface analysis, EDS and magnetic properties results respectively.

4.1 – ROUGHNESS RESULTS

4.1.1 – Optical microscope and roughness results for C821 roughing condition

Hard materials can be machined with the use of electrical discharge machining having a removal mechanism based on ablation [42]. The roughing condition (C821) is the most aggressive condition. An optical microscope LEICA DM 4000M was used in order to obtain pictures from the machined surface with the roughing condition (C821). Figure 26 exhibits one optical microscope with 100 times ampliation obtained for a blade of Nd-Fe-B machined with the roughing condition. The pattern is composed of little dots, these dots are spheres of Nd-Fe-B which remained attached to the surface. These spheres are formed during the machining process when the temperatures are extremely high, and the material melts and spherodizes before solidification. Part of the formed spheres

remains attached to the surface piece. As expected, this condition has provided the worst roughness results due to their high thermal energy [43].

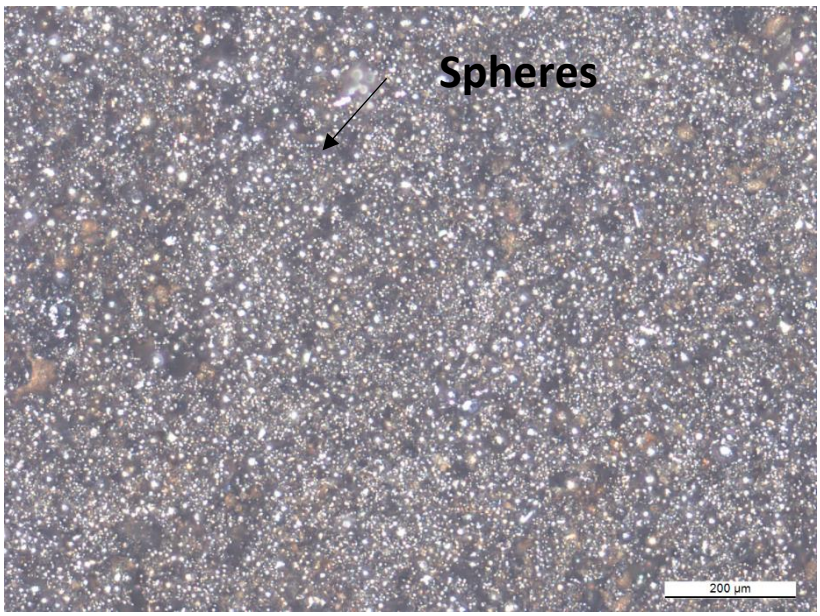

Figure 26 - 100 times magnetization of Nd-Fe-B blade machined by roughing condition.

The data obtained regarding roughness analysis is plotted in Figure 27 along with one of the surface roughness profiles treated with Taylor il20 Surf. It is important to note that each column in Figure 27a represents one roughness parameter, and the red bars represent the standard deviation for the measurement that can also be found in Figure 27b. It's also important to notice that the scales for the roughness profiles are different for each sample.

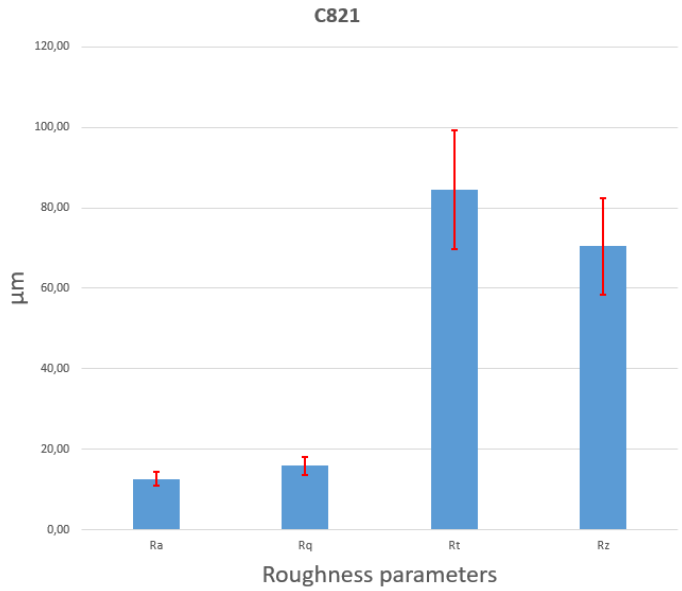

(a)

Machining condition: C821		
Roughness parameter	Average (µm)	Standard deviation (µm)
Ra	12,66	1,74
Rq	15,91	2,20
Rt	84,47	14,76
Rz	70,45	11,95

(b)

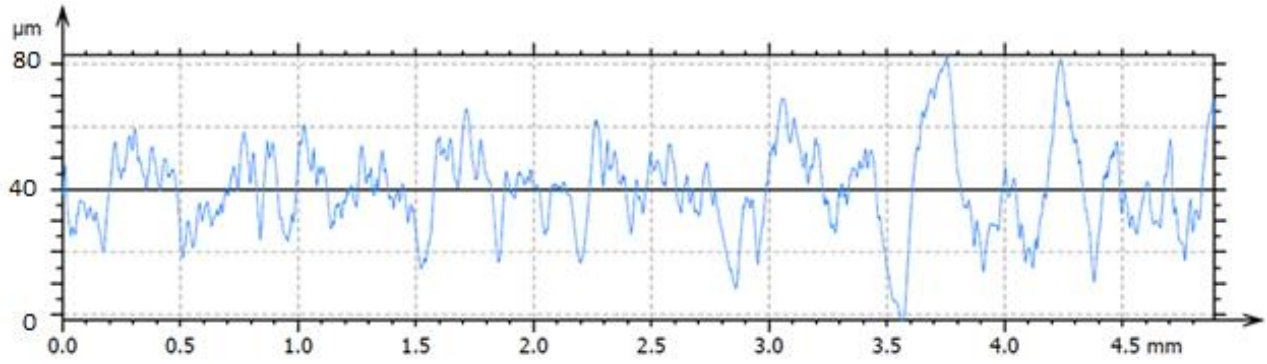

(c)

Figure 27 - (a) Chart with roughness parameters, (b) roughness parameters presented in a table format and (c) surface roughness profile.

For further applications, the imperfections on the surface need to be removed. By having such a roughness value, the magnet is subject to several different problems. If the surface has a high roughness values, it will lead to faster oxidation, since water and other impurities can remain in the depths of the roughness profile [44]. This surface would also need more coating material, so for the coating of the magnet this surface would need to be removed with further machining. In addition, the magnets properties are likely to suffer an impact due to the irregularities of the surface.

4.1.2 – Optical microscope and roughness results for C822 semi-fining condition

Figure 28 is an image with 100 times magnification taken with an optical microscope from the sample machined by C822 condition. It's possible to note how the surface differs from the previous condition, as this surface was not covered by the same pattern as in the previous condition. However, it still has some dotted pattern, but also now remolten material, which will be shown in pictures taken with SEM in the next sections.

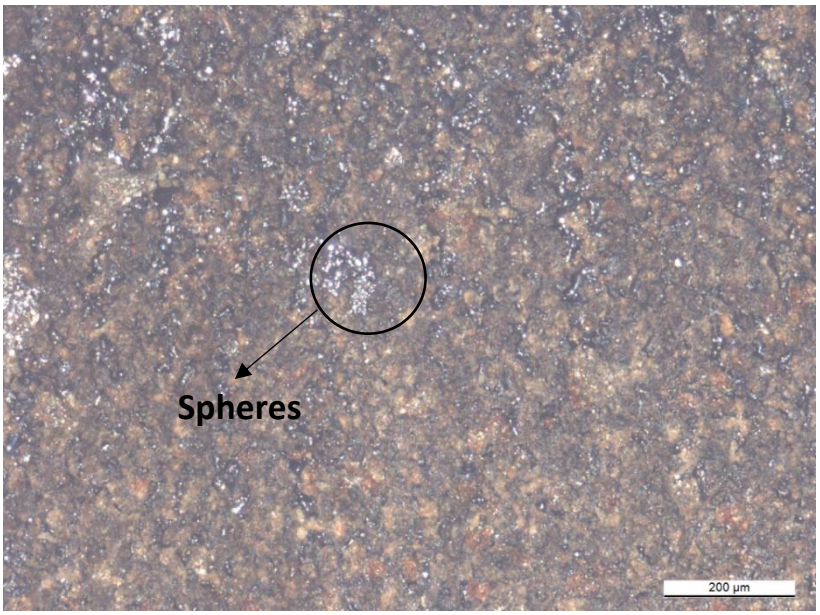

Figure 28 - Optical microscope image of surface machined by C822 machining condition.

The roughness parameters regarding this machining condition were collected and are presented in Figure 29 along with a surface roughness profile obtained for one of the surfaces.

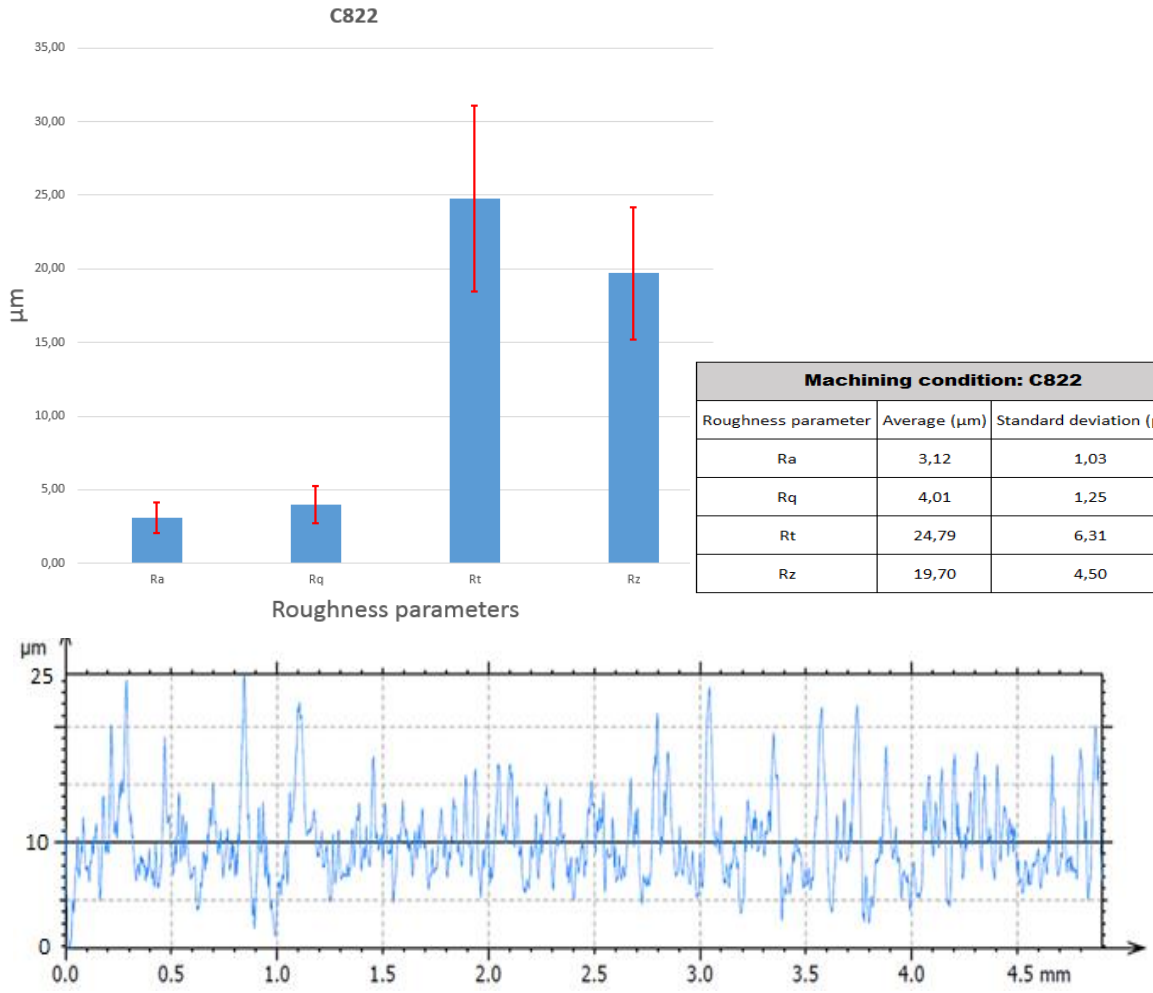

Machining condition: C822		
Roughness parameter	Average (µm)	Standard deviation (µm)
Ra	3,12	1,03
Rq	4,01	1,25
Rt	24,79	6,31
Rz	19,70	4,50

Figure 29 - Roughness results for C822 machining condition.

The results have shown that for this condition there was a reduction in average roughness (Ra) from 12.66 µm to 3.12 µm, when compared to the first condition. This is expected since this condition is much less aggressive than the previous, and according to other works regarding EDM, the higher the energy delivered the more detrimental will be the process for the surface [45]. This surface would also need to be removed for application, because it has thermal cracks as it will be shown in next sections and the presence of the spheres is still a problem for coating processes and magnetic properties for examples [46, 47]. A compilation of all the roughness parameters for all the conditions will be presented in the end of this section to compare the roughness parameters for all the machining conditions.

4.1.3- Optical microscope and roughness results for C823 finishing condition

Figure 30 shows the optical microscope image obtained with 100 times magnification obtained for one of the samples machined by C823 machining condition. It has a similar visual aspect with surfaces machined with semi-finishing condition (C822), the whole surface is covered with the same pattern presented in Figure 26. The energy delivered by finishing conditions is much smaller when compared to semi-finishing and roughing conditions, therefore the damage in the surface is less detrimental.

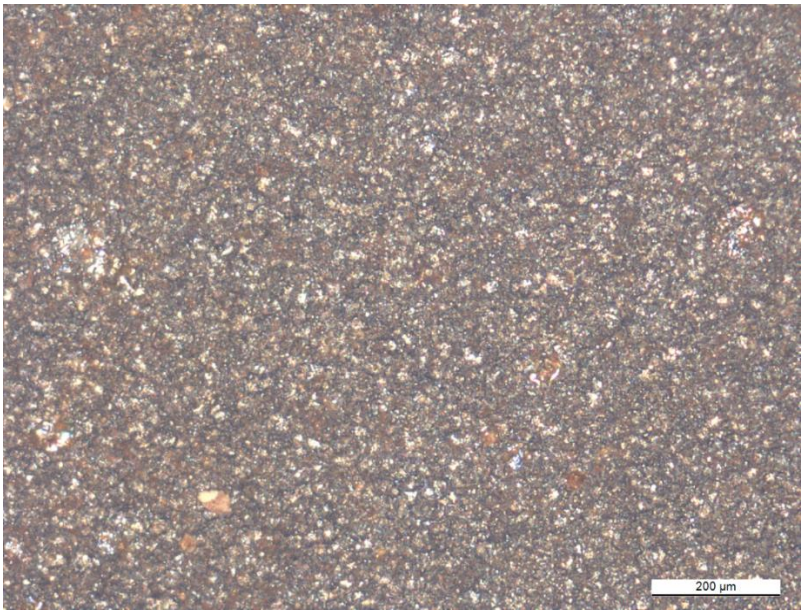

Figure 30 - One hundred times magnification for samples machined with finishing condition C823.

The roughness parameters results obtained for this condition are shown in Figure 31 along with a surface roughness from one of the samples. The results for this condition are even better than the previous condition, this happens because of the reduction of the energy input in this condition. The advantage of the machining with the fining conditions is that the surface is less damaged, which means a smaller impact on magnetic properties and a less fragile magnet [48].

However, as a disadvantage its possible to mention that this machining condition takes more time, which implies in a less productive process.

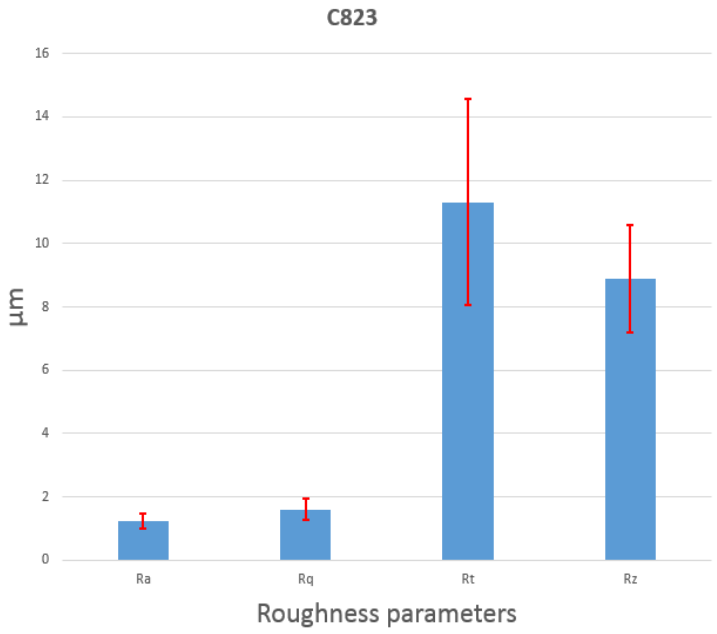

Machining condition: C823		
Roughness parameter	Average (µm)	Standard deviation (µm)
Ra	1,24	0,23
Rq	1,61	0,32
Rt	11,31	3,26
Rz	8,90	1,69

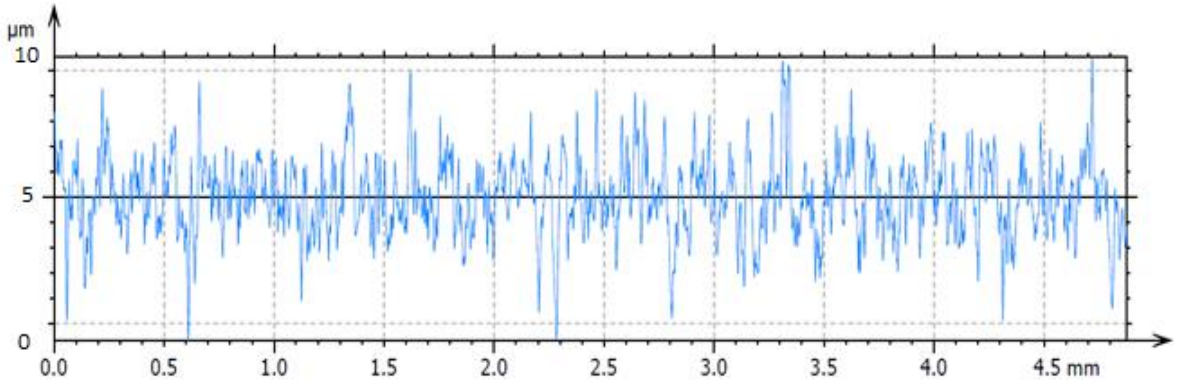

Figure 31 - Roughness parameters plotted in graphic, table and roughness profile for surface machined with C823 condition.

When compared to the previous semi-finishing condition (C822), the roughness average value decreased from Ra = 3,12 µm to Ra = 1,24 µm. And when compared to the most aggressive condition, the roughness average dropped from Ra = 12,66 µm to Ra = 1,24 µm, which means a reduction of approximately 90% in this roughness parameter from one condition to another. This condition can be considered as an intermediate condition between the rough and finishing conditions.

4.1.4 - Optical microscope and roughness results for C824 finishing condition

Figure 32 was taken with an optical microscope using 100 times magnification. The same pattern observed in Figure 30 can be also observed in Figure 32. This indicates that the two finishing conditions have a pretty much similar effect on rugosity regarding Nd-Fe-B samples. Since the two finishing conditions produced very similar results, they could be use interchangeably. For all conditions the remaining surface will not be good for the magnet, coating and mechanical properties of the magnets. As a result, all the surfaces would need pos processing for an industrial application.

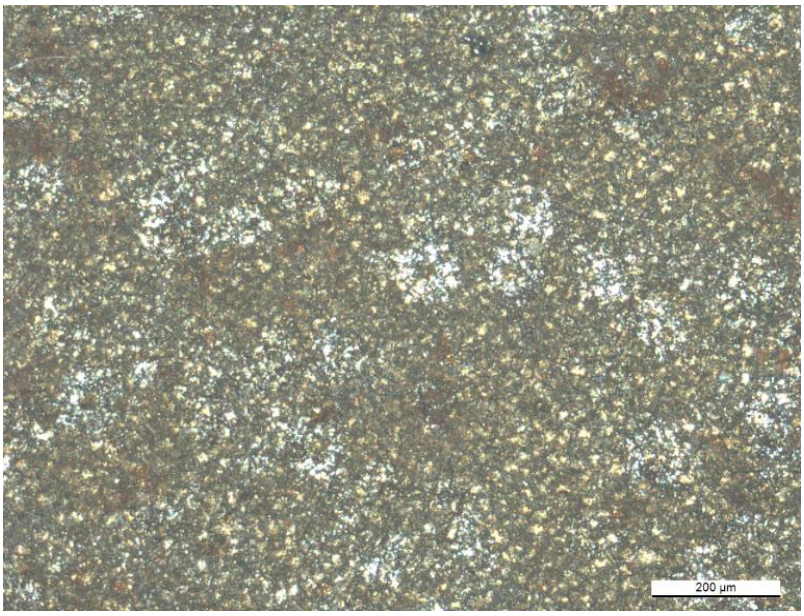

Figure 32 - MO image for last condition with 100 times magnification.

Figure 33 exhibits roughness parameters obtained with Taylor Surf il20 rugosimeter along with a surface roughness profile.

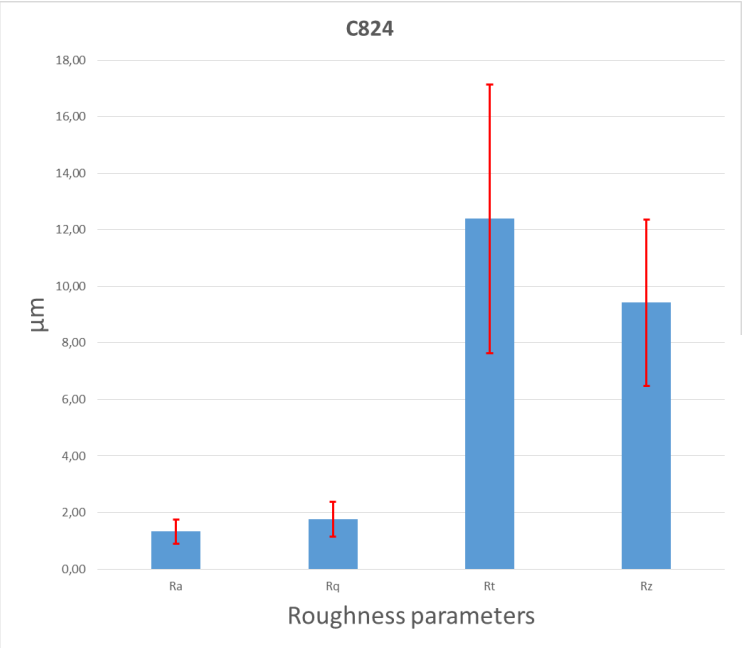

Machining condition: C824		
Roughness parameter	Average (µm)	Standard deviation (µm)
Ra	1,32	0,44
Rq	1,76	0,61
Rt	12,39	4,74
Rz	9,42	2,95

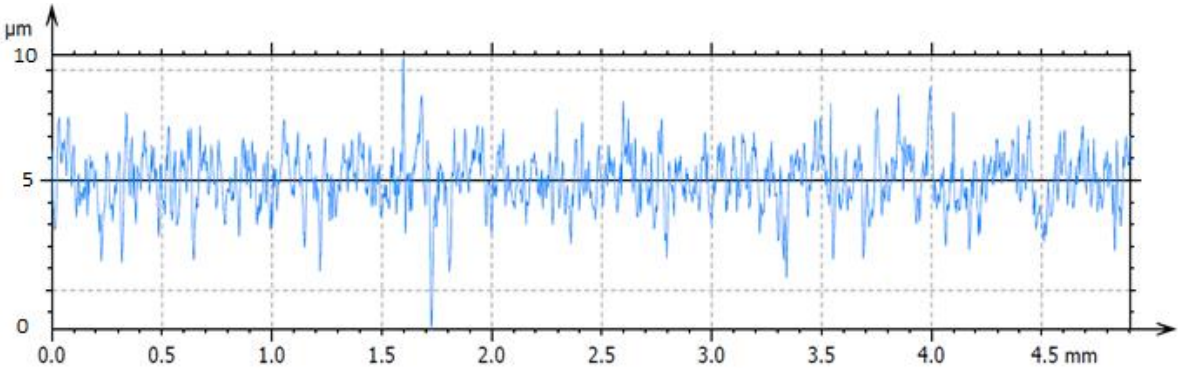

Figure 33 - Roughness results for last finishing condition C824.

When compared with the C823 condition, the roughness averaged varied from Ra = 1,2420 µm in the previous condition and Ra = 1,3212 µm for this condition.

4.1.5 – General roughness results between all machining conditions

Figure 34 along with Table 3 were plotted in order to better understand the difference in roughness parameters obtained for all four conditions in the same scale.

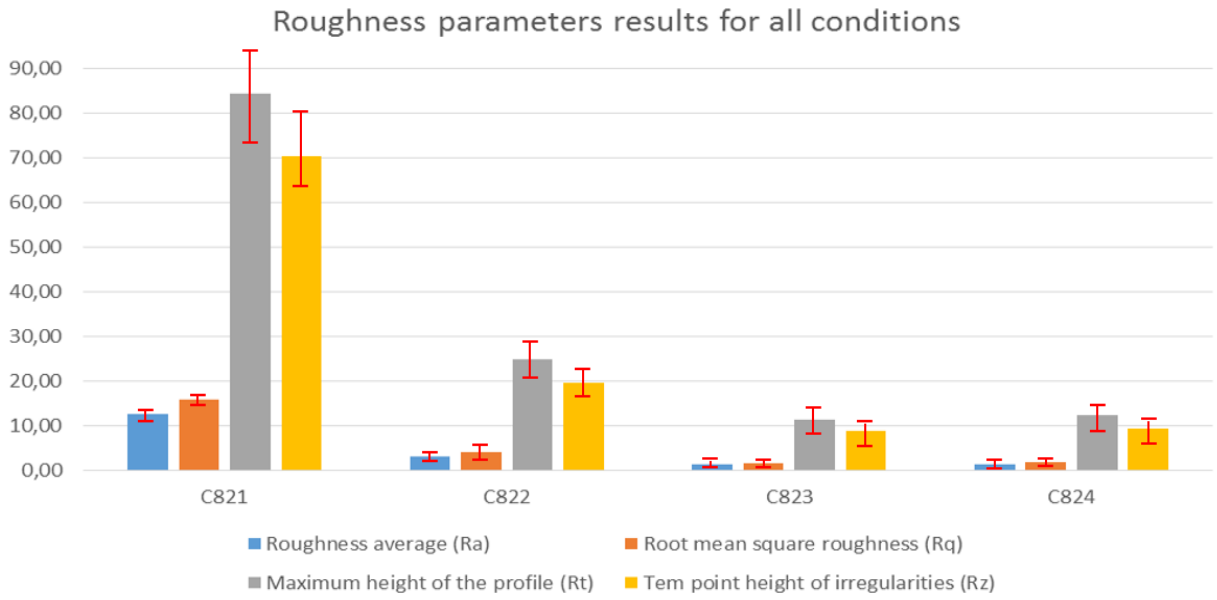

Figure 34 - Comparative roughness between machining conditions.

Table 3 - Compiled roughness results.

	Machining conditions							
Roughness Parameters	**C821 (7 A, 24 µs, 14 µs) (Roughing)**	**σ**	**C822 (3 A, 05 µs, 04 µs) (Semi-finishing)**	**σ**	**C823 (2 A, 31 µs, 31 µs) (Finishing)**	**σ**	**C824 (2,5 A, 31 µs, 01 µs) (Finishing)**	**σ**
Roughness average (Ra)	12,66	1,74	3,12	1,03	1,24	0,23	1,32	0,44
Root mean square roughness (Rq)	15,91	2,20	4,01	1,25	1,61	0,32	1,76	0,61
Maximum height of the profile (Rt)	84,47	14,76	24,79	6,31	11,31	3,26	12,39	4,74
Ten point height of irregularities (Rz)	70,45	11,95	19,70	4,50	8,90	1,69	9,42	2,95

In general, a reduction in the energy input will provide a better surface quality. And on the other hand, an increase in the energy input (which can be translated in thermal impact) will also result in an increasing roughness, sphere formation and damage on the surface. The roughness parameters increased when the machining parameters such as current and Time-on were higher, as it can be seen for the roughing and semi-roughing condition. The last two conditions have produced very similar results, this was expected because their

similarities regarding machining parameters such as current and Time-On, despite the fact that they have a very different Time-Off machining parameter as can be observed in Table 1 and 3.

The following schematic in Figure 35 represents that the bigger the energy input, the bigger it will be the roughness parameters as well as the damage in the surface and surface defects. As observed by Amorim et al, an increase on the energy input delivery to the cutting zone will intensify the removal of the material and will have bigger impact on surface integrity. In the WEDM, the material diffusion processes between work-piece and wire electrode are very intense due to the high temperatures (over 8000 K) that normally occurs during the discharges [49]. In general, the higher the current the higher it will be the resulted roughness, presence of tracks, pores, re-molten material and other surface defects. The presence of this damaged surface is not desired specially for magnetic materials, the magnetization or demagnetization starts by the surface, therefore the minimum damage to the surface can have an impact on the demagnetization of magnetic materials. And the opposite is also true, the smaller the energy input the smaller it will be the roughness, the surface will be less damaged and it will contain less surface defects.

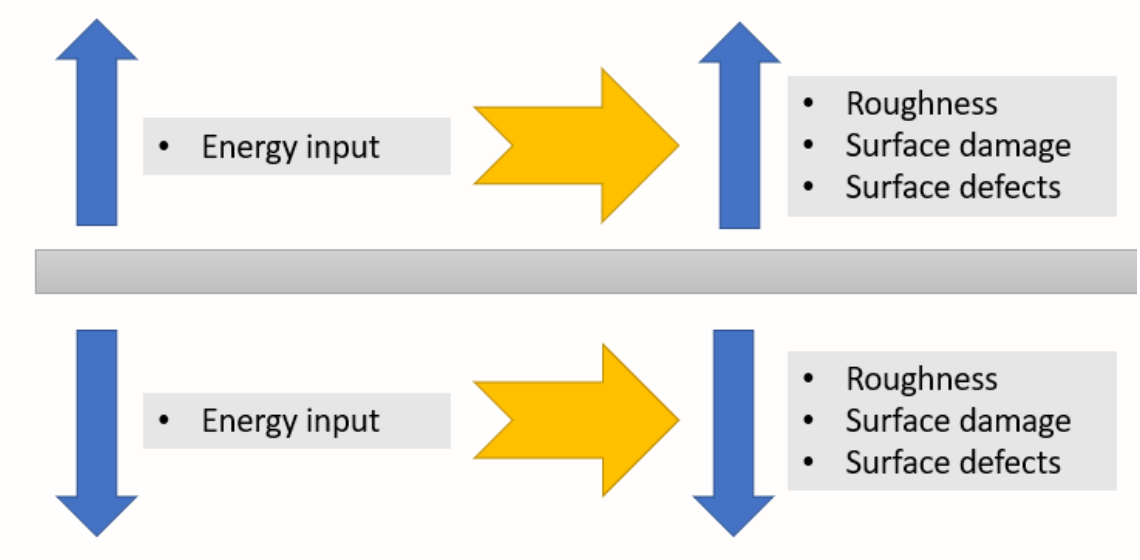

Figure 35 - Relationship between energy input and surface quality.

Next section will present results with scanning electron microscopy that will give a better image on the sphere-shaped detritus and the other characteristics of the surfaces machined with WEDM for the conditions presented in this work. In addition, the section will also provide information regarding the

chemical composition of the surfaces, this will help to understand the results of magnetic properties that will be present in the last section of this chapter.

4.2 – SEM AND EDS RESULTS

4.2.1 - Surface morphology generated by C81 roughing machining condition

The spheres are formed due solidification of material after ablation. In further images it will be also possible to observe that the ablation effect also occurs even in spheres that are over other spheres. Both hollow and solid sphere-shaped chips remain attached to the surface after machining. In Figure 36, a magnification of 1000 times is shown for the same sample and same characterization technique. It is possible to understand that the sphere-shaped pattern is actually composed of several layers of sphere chips. In Figure 36 it can

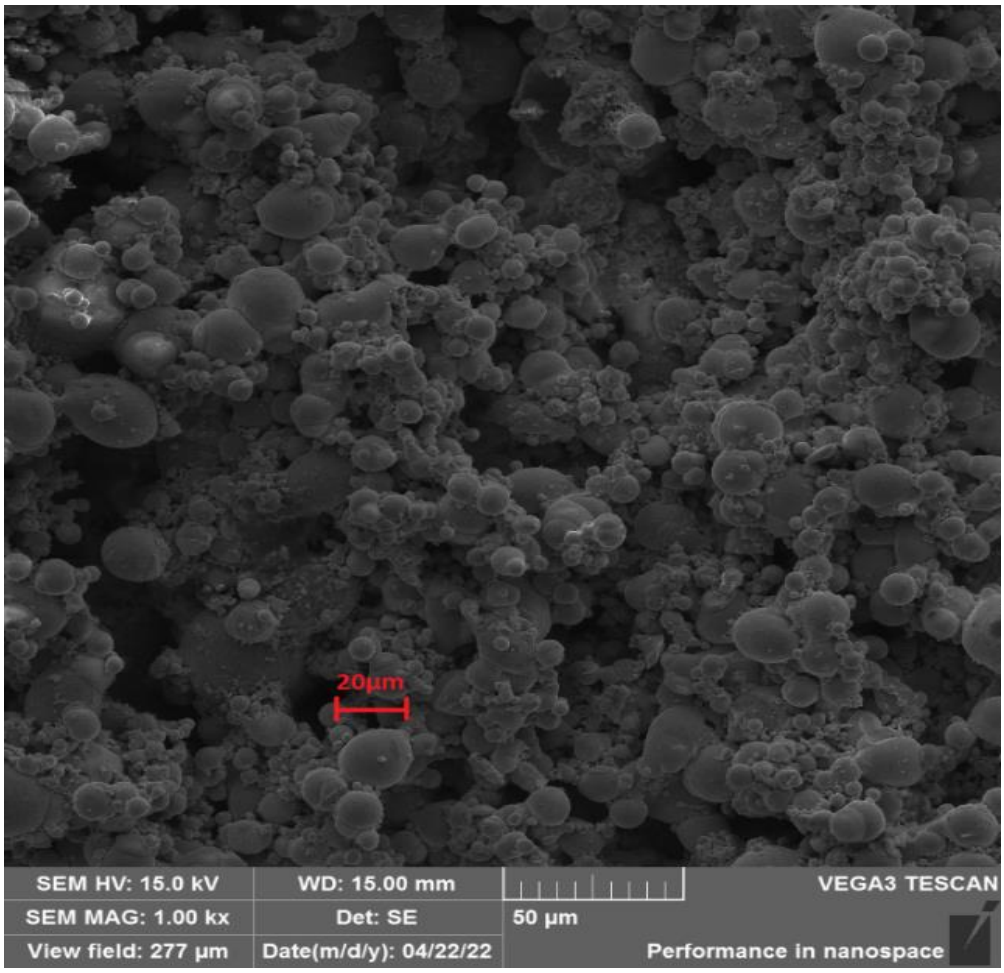

Figure 36 - 1000 times magnification SE image.

be observed that the chips have different particle sizes, with some of them having a diameter larger than 20 µm.

The presence of this layer composed of spheres will have various consequences for the magnets. One consequence would be use of more coating material, which would make the processing of producing the magnet more expensive. Another consequence for the magnet is the drop on its magnetic properties such as remanence and coercivity. So in an industrial application this layer formed of spheres would need to be removed in other to obtain a better magnet [50, 51].

In Figure 37, it is possible to observe a large amount of remelted material and thermal cracks formed due to the highly aggressive temperature cycle. This cycle creates internal tensions that end up cracking the surface. In addition, sphere chips that were not completely removed during machining got stuck in the molten material and became stress points.

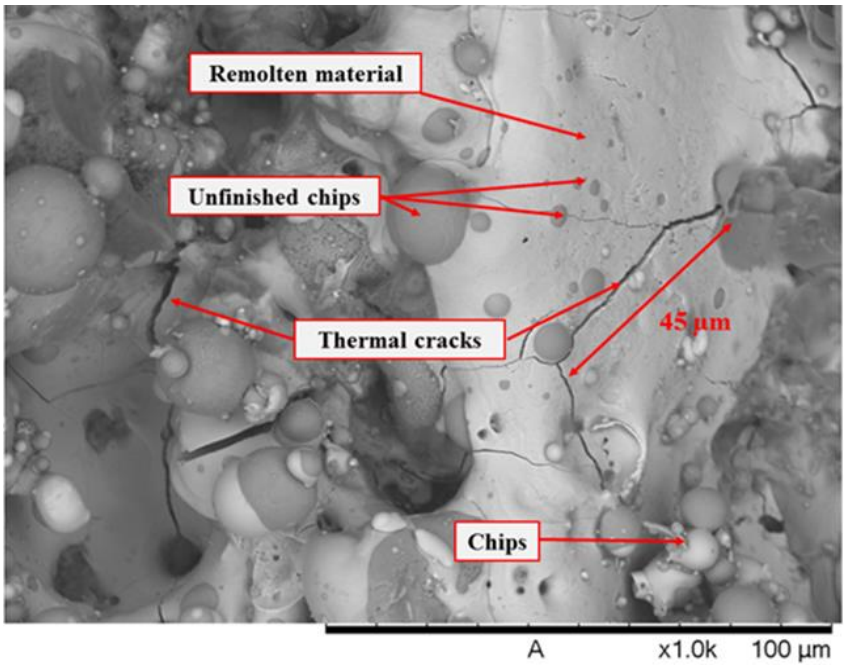

Figure 37 - Presence of surface defects on Nd-Fe-B sample after machining obtained with TM3030 Microscope.

This is not desirable, especially for highly reactive materials such as Nd-Fe-B, as it provides a starting point for corrosion mechanisms to take place, thereby reducing the magnet's life under harsh environments. The presence of these characteristics will have a negative influence, especially for magnets with

a high surface-to-volume ratio, such as submillimeter magnets [52]. This happens because as a multi-phase, complex ternary system, Nd-Fe-B solidifies incongruently in the heat-affected zone, leading to a non-homogeneous distribution of phases. This, in turn, causes an unbalance in the chemical composition on the surface of the magnet that can cause substantial losses in the magnetic properties, especially in submillimeter magnets [53]. One should minimize the molten volume in order to minimize this detrimental effect.

Figure 38 shows the moment where spheres started to be formed on top of previously formed spheres chips. The spheres are formed due to the high energy input, which is an intrinsic characteristic of electrical discharge machining. After one discharge the spheres are created, however they solidify fast and the following discharge creates another sphere over the recently formed sphere. One can also see that the spheres sizes vary significantly, going from less than 1 μm to over 30 μm as shown in Figure 38 Since the roughing condition is the more energetic, this sphere formation phenomena is more prominent in this condition, specially the formation of larger spheres and spheres over spheres.

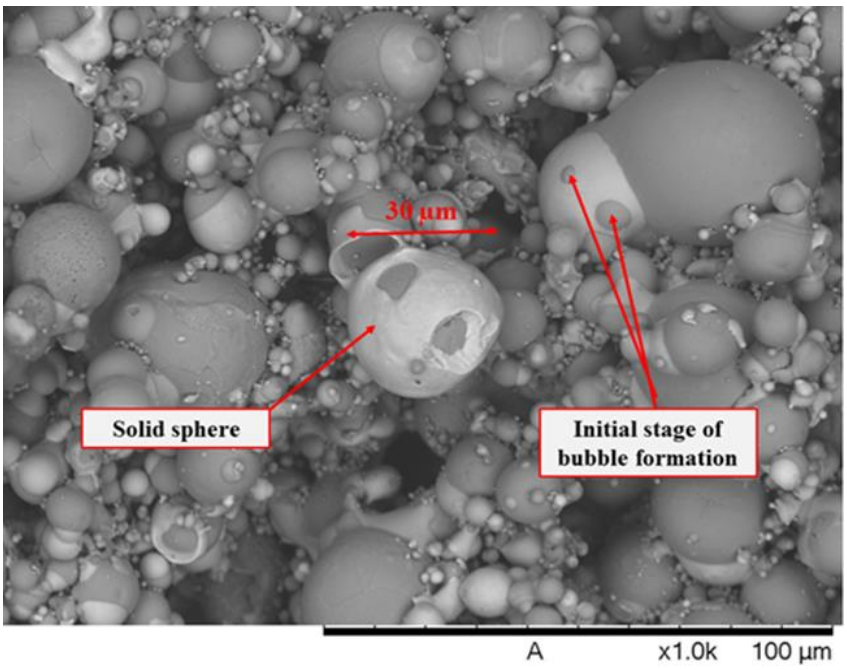

Figure 38 - Debris remain attached to the surface after machining.

Figure 39 shows a BSE image from the rough machined surface. The back-scattered electron technique also provided some information regarding sample composition. The darker areas correspond to lighter elements such as free iron, a soft magnetic phase, not desired. On the other hand, the lighter areas correspond to heavier elements such as neodymium-rich phases, non-ferromagnetic. This segregation happens during solidification, due to high temperatures reached during machining and it has an impact on magnetic properties as it will be discussed in next sections.

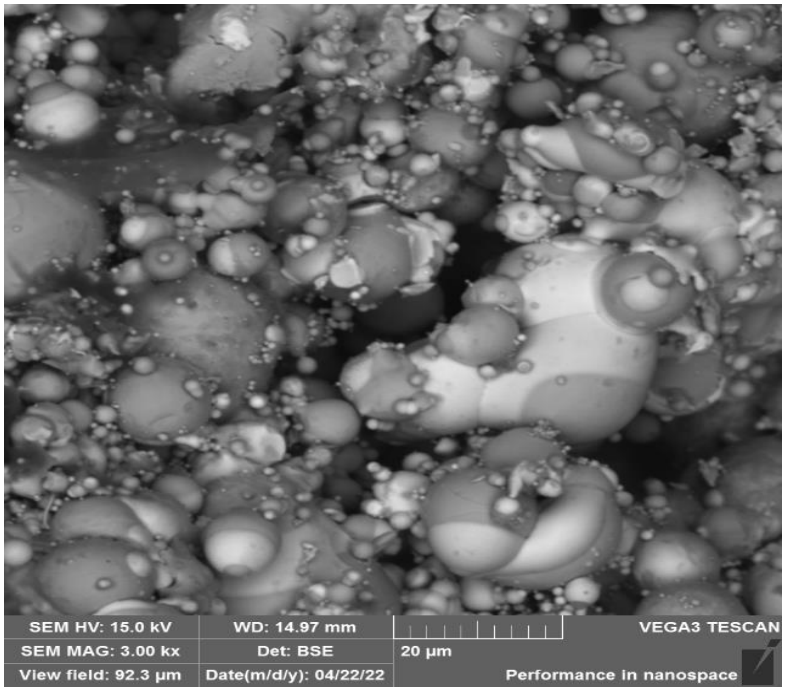

Figure 39 - BSE image with 3000 times ampliation.

4.2.2 – EDS results for C821 roughing machining condition

An energy dispersive spectroscopy (EDS) was conducted in order to better understand the chemical composition of the surface generated by C821 rough machining condition. A region was analyzed with 3000 magnification and mapped regarding its chemical composition. Figure 40 represents (a) the EDS image of this region and (b) the chemical composition map.

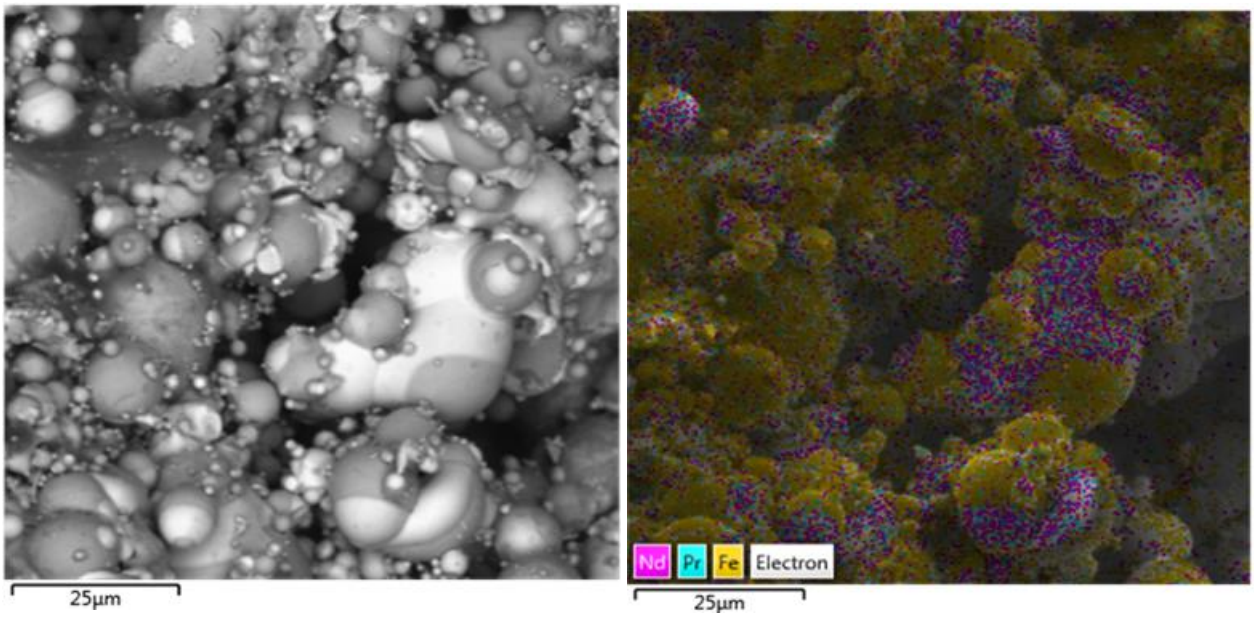

(a) *(b)*

Figure 40 - (a) BSE image for mapped region and (b) chemical map.

It's possible to observe that purple areas have a predominance of neodymium and praseodymium, meanwhile yellow areas present iron concentration. These images indicate that during machining the main phase of $Nd_2Fe_{14}B$ disintegrates into two phases, having different compositions. This phenomenon was very present for roughing machining and not so intense for semi-finishing and finishing machining conditions.

4.2.3 - Surface generated by C822 semi-finishing machining condition

A scanning electron microscope was also used in order to study the remained Nd-Fe-B surface obtained with the semi-finishing machining condition. Figure 41 shows a 500 times ampliation image of the resulting surface. The roughing condition produced a surface covered with spheres, which did not happen for the surface machined with the semi-finishing machining condition. This difference happens because the energy input provided by the previous roughing condition is much higher than this one. The pattern now is formed by remolten material, craters, cracks and much smaller debris as indicated in Figure 39. The energy input while machining has a direct impact on the sphere formation

and size, so less energetic machining conditions will generate smaller debris sizes and a less damaged surface.

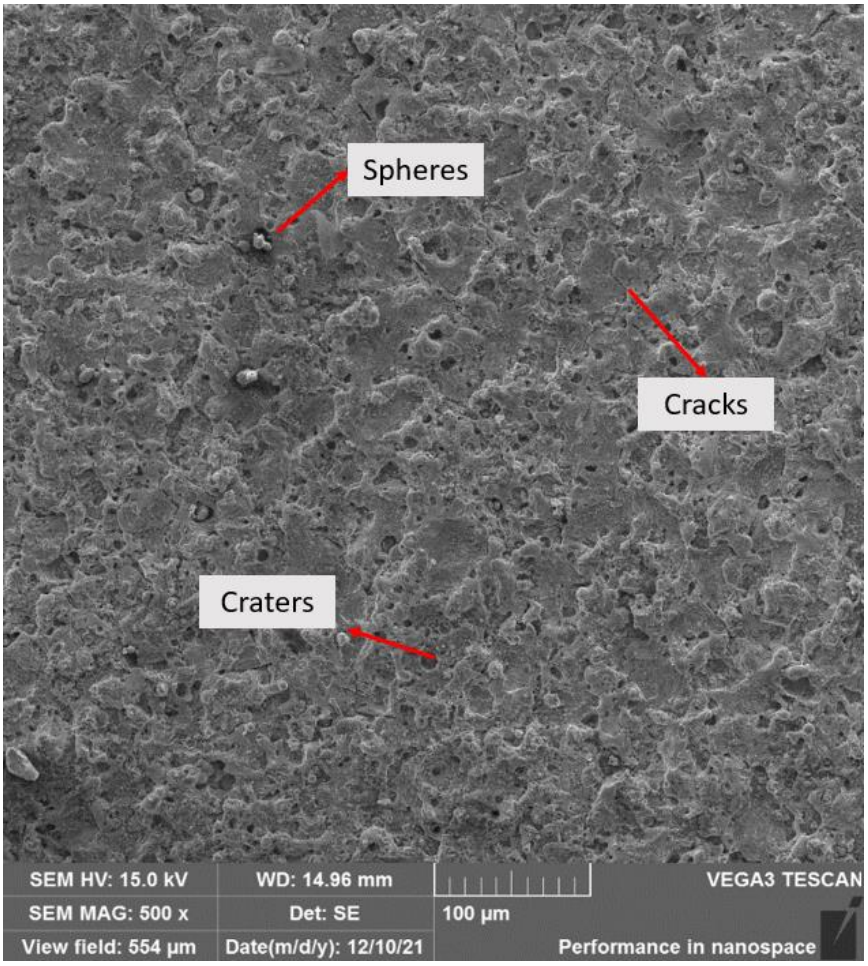

Figure 41 - Surface generated with semi-finishing machining condition.

4.2.4 - EDS results for C822 semi-finishing machining condition

In order to study qualitatively the chemical composition variation of the surface machined by condition C822, an EDS analysis was made for the surface generated by this machining condition. Figure 42 (a) shows the region studied with a 3000 times magnification, and (b) shows the map of elements. The previous rough condition (C821) showed a much more damaged surface, where the surface itself was covered with this layer of segregated free iron and neodymium rich spheres. For this semi-finishing condition, the surface also suffered segregation of elements, but the sphere formation was much less pronounced because of the lower thermal impact. The lighter areas still correspond to areas with Nd, Pr dominance, meanwhile the yellow areas indicate

iron predominance. Even with a less intense dissociation, this surface is still not ideal for hard magnetic properties, once the microstructure was deeply altered.

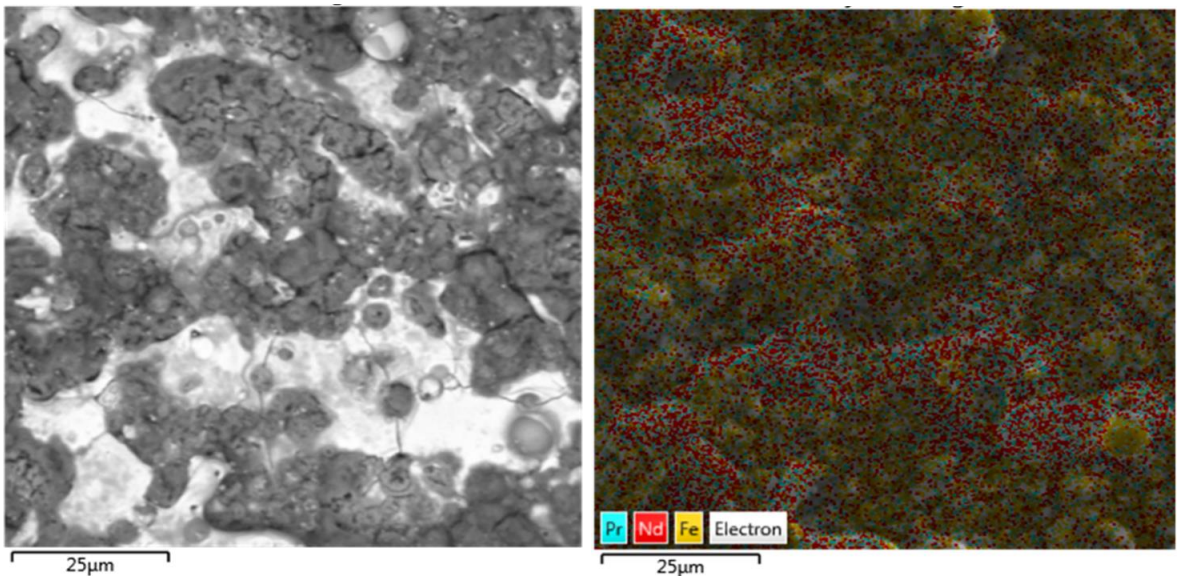

(a) (b)

Figure 42 - BSE image obtained for EDS analysis.

Even though this surface presents a less damaged image than the surface presented for the roughing condition C821, it still has a lot of defects and it would not be useful for an industrial application. First it has cracks, spheres attached and these defects can lead to surface crack propagation. In addition, the two phases are not good for the magnet, ideally the magnets would be all made from the primary phase with a Nd-rich phase on the grain boundaries and junctions. Therefore, for an industrial application this remelted layer would be also removed in order to optimize magnetic properties and mechanical integrity [54].

4.2.5 - Surface generated by C823 finishing machining condition

The finishing condition C823 has 2 A for current, 31 µs for time on and 31 µs for time off being considered as a finishing condition. These set of parameters will create a less damaged machined surface which is shown in Figure 43. As it was just discussed, even though the surface looks even better now, it would still not be useful for industrial applications [55]. Therefore, it's possible to say that

the thermal impact is too high even for the finishing machining condition here presented.

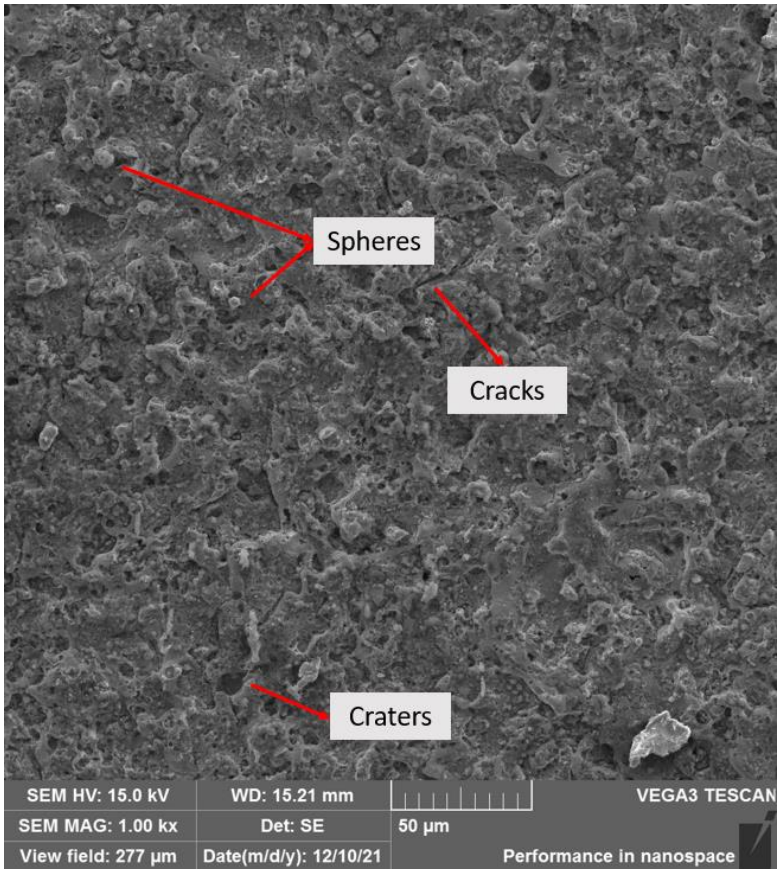

Figure 43 - Surface generated with finishing condition.

As it can be seen, this surface is composed of remolten material with less and smaller spheres when compared to rough machining condition. However, this finishing condition produced very similar results as the semi-finishing machining condition. This happens because the parameters are very similar, with semi-finishing machining condition having 3 A for current, 05 µs for time on and 04 µs for time off.

The machining defects found in Figure 41 can be also seen in Figure 43 with one thousand times magnification image showing craters, cracks and remained spheres all along the surface.

4.2.6 - EDS analysis for C823 semi-finishing machining condition

Since the parameters for this condition are not so different than the ones for the semi-finishing conditions, the EDS results are also very similar. The whole surface is covered with a homogenous distribution of areas with higher concentration of neodymium/praseodymium and other areas with higher frequency of iron. The disproportion phenomena are also observed for this condition, however with less intensity when compared to semi-finishing and specially with rough machining. Figure 44 (a) indicates an image obtained with 3000 thousand times ampliation of the surface and (b) its chemical map composition obtained with energy dispersive spectroscopy.

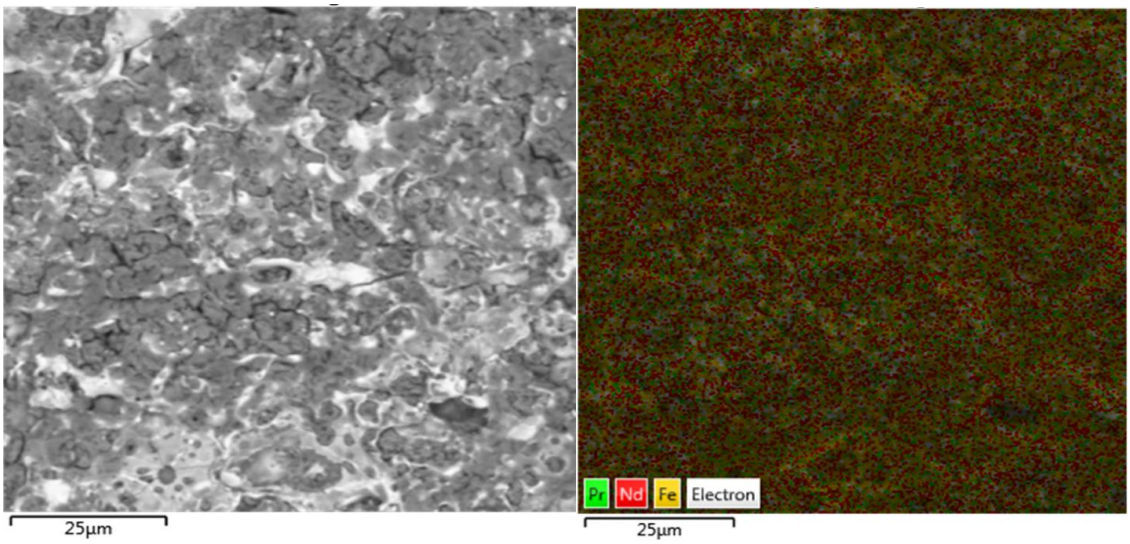

Figure 44 -(a) BSE image and (b) chemical map for sample machined with finishing condition C823.

4.2.7 - Surface generated by C824 finishing machining condition

The last machining condition studied in this work has 2.5 A for current, 31 µs for time on and 01 µs for time off. Since these parameters are very similar to the ones used in the previous finishing machining condition, the results are also very similar as expected. Figure 45 shows the same pattern observed before for the semi-finishing and the other finishing machining condition. All the machining defects can be also found in this surface. When comparing just the two finishing

conditions, it's possible to note that the parameter time off played a minor role on the surface generated.

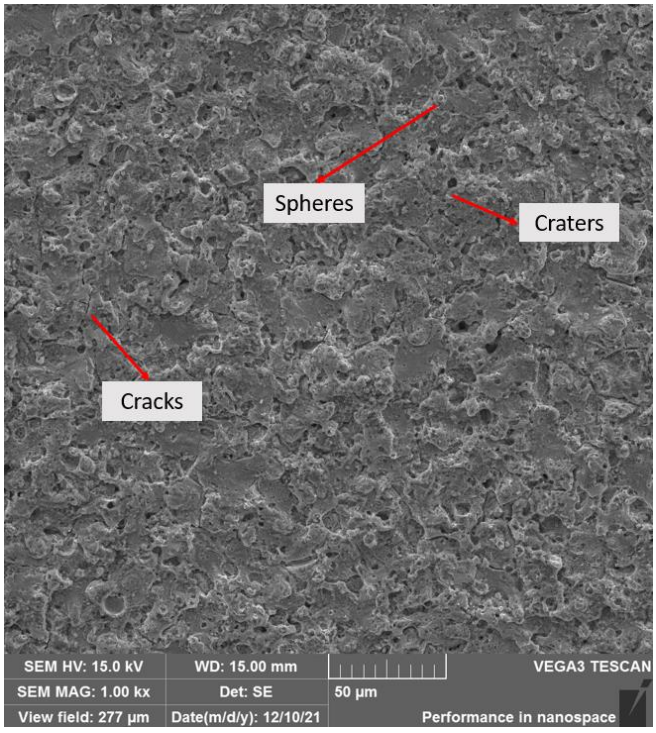

Figure 45 - SE image of surface after machining process with finishing condition C824.

4.2.8 - EDS analysis for C824 finishing machining condition

As expected, because parameter similarity, the results for EDS for the finishing condition C824 are pretty much the same as the ones for the two previous conditions. Figure 44 (a) shows the image obtained of the surface with three thousand times magnification and (b) the chemical map regarding the same area. The two major areas containing iron and Nd/Pr are found all along the surface, indicating that the disproportion had a very similar intensity when compared to the semi-finishing and C823 finishing machining condition. Since the results are practically the same for both the finishing conditions, it was decided for the use of a 5000 times amplification for this last finishing condition analysis in order to go further with the investigation on the surface composition. It is important to point that during the analysis it was observed that the 3000 times amplification would bring basically the same image, so in order to go further with

the investigation and bring new results, the 5000 times amplification was chosen and is presented below in Figure 46.

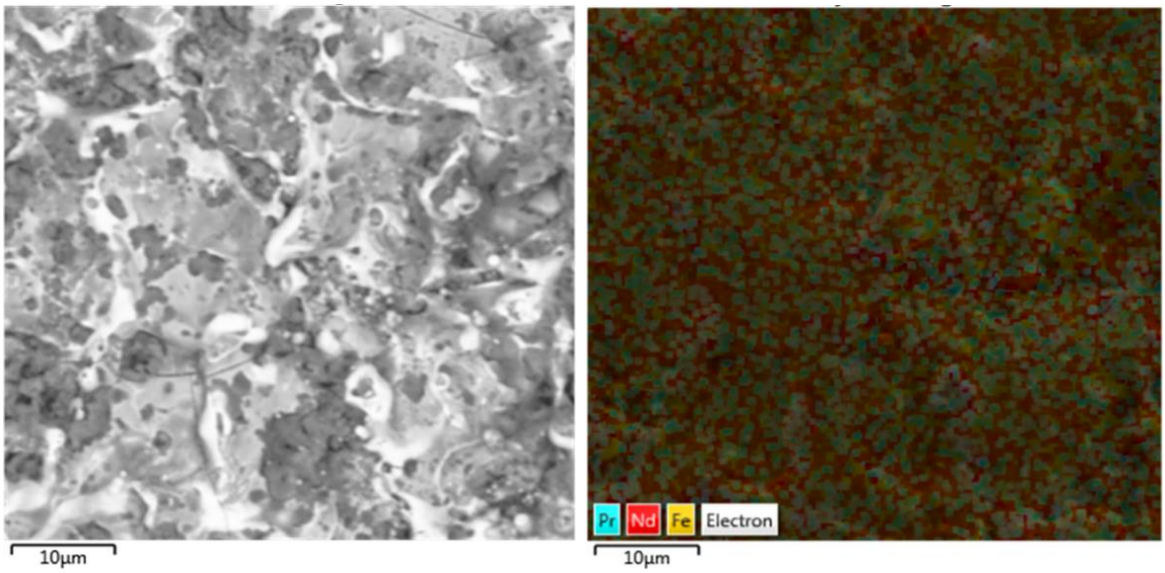

(a) (b)

Figure 46 - (a) BSE and (b) chemical map for sample machined with finishing condition C824.

The SEM analysis of the surfaces machined with different conditions have shown that even for the finishing conditions (C823 and C824) surface defects are still present. The main difference was the intensity of the sphere formation and also the segregation of the main phase ($Nd_2Fe_{14}B$) in a Nd-rich phase and an iron rich phase. Regarding the surface quality, all the samples would still need to be submitted to post-processing in order to be able to be coated and improving magnetic properties. The machining time is of course higher for finishing conditions, since they cut with less energy and therefore more time is needed. However, measuring the machining time was not in the scope of this work and another study would be need to understand if it would be the best machining condition option in terms of productivity. Next section will provide the results obtained for the cross-section layer which will complement the results displayed in this section and it will also help to understand the results of magnetic properties which will be presented in the end of this chapter.

4.3 – CROSS SECTION LAYER RESULTS

It's possible to observe the impact from the cut towards the bulk with pre-polishing technique [56]. In order to study the effects not only on the surface but also towards the bulk of REE's magnets machined with WEDM, the pre-polishing methodology described previously. The samples then were analyzed with Vega3 Tescan scanning electron microscope using BSE and SE techniques and the results are presented in next pages.

4.3.1 – Cross section layer for C821 roughing machining condition

Figures 47 shows the results obtained for a sample machined with the roughing condition. The images show a layer of sphere-shaped detritus that remained attached to the surface.

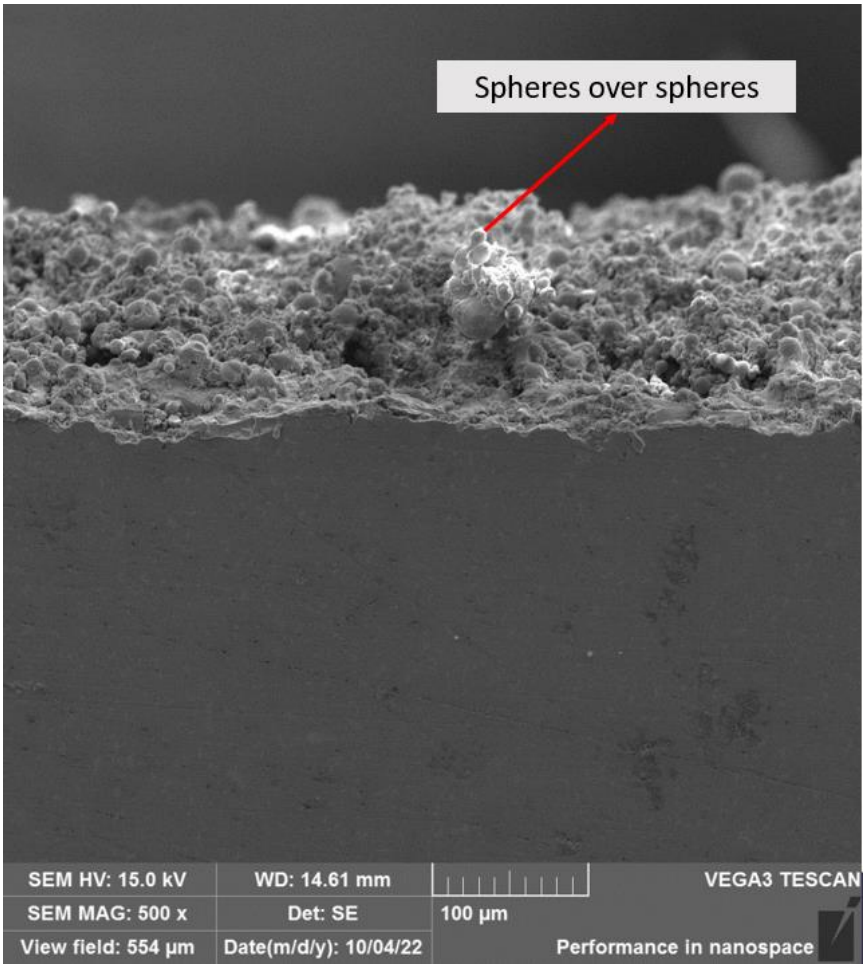

Figure 47 - Cross-section for sample machined with roughing WEDM.

It is not possible to determine how thick is this layer covering the surface, however it is possible to observe from another angle the sphere over sphere formation that happens when roughing machining is used.

Figure 48 is a BSE image of the same sample with one thousand times ampliation. In this image is possible to observe the presence of cracks on the material on the machined surface towards the bulk. This microcracks can lead to whole grain removal if the intensity of the cracking is high enough.

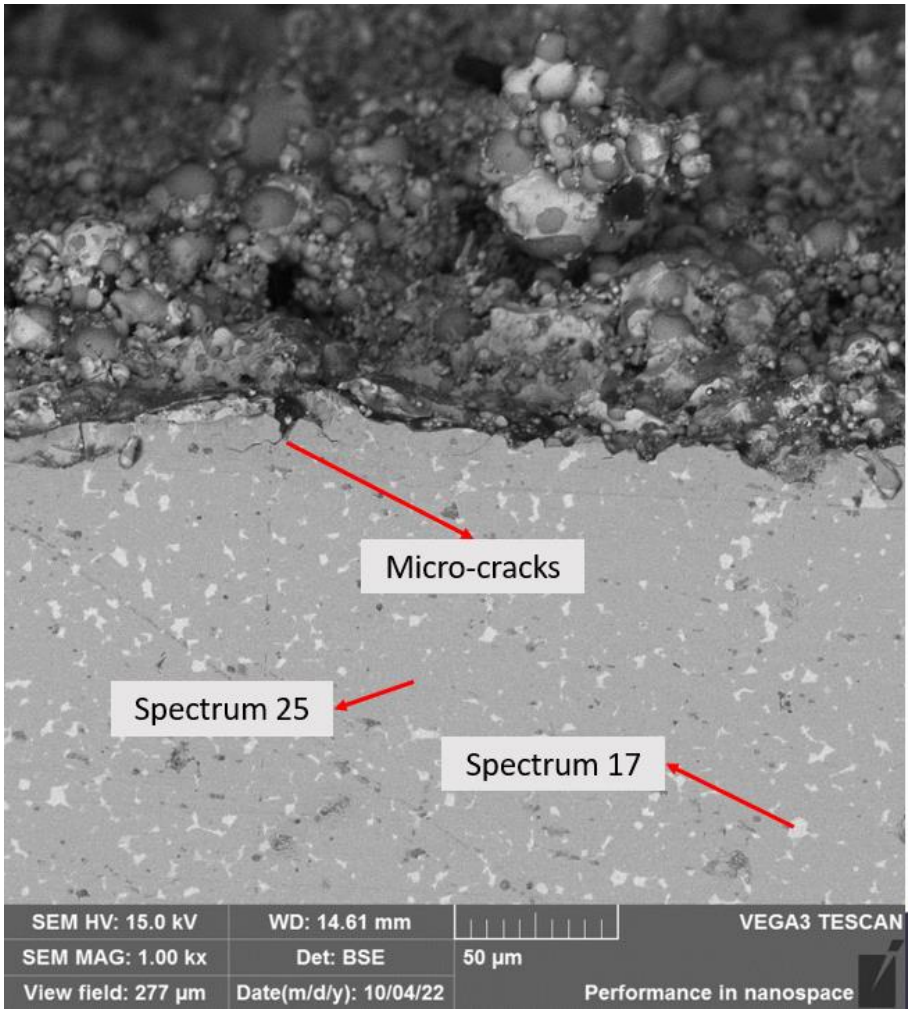

Figure 48 - Cross sectional layer image with 1000 times magnification.

It's also possible to observe the main phase of $Nd_2Fe_{14}B$ and Nd-rich areas presented with lighter color. It's clear that the material was not substantially affected towards its bulk, which indicates that the WEDM can be very damaging to the surface, but has no affect towards the bulk of the material and therefore no impact on the magnetic properties of the magnets. Spectrum 25 represents the main phase $Nd_2Fe_{14}B$ with a gray color, and spectrum 17 represents the Nd-Rich

region, showing a brighter color when analyzed by BSE technique. Spectrums 25 and 17 are displayed in Figures 49 and 50 respectively.

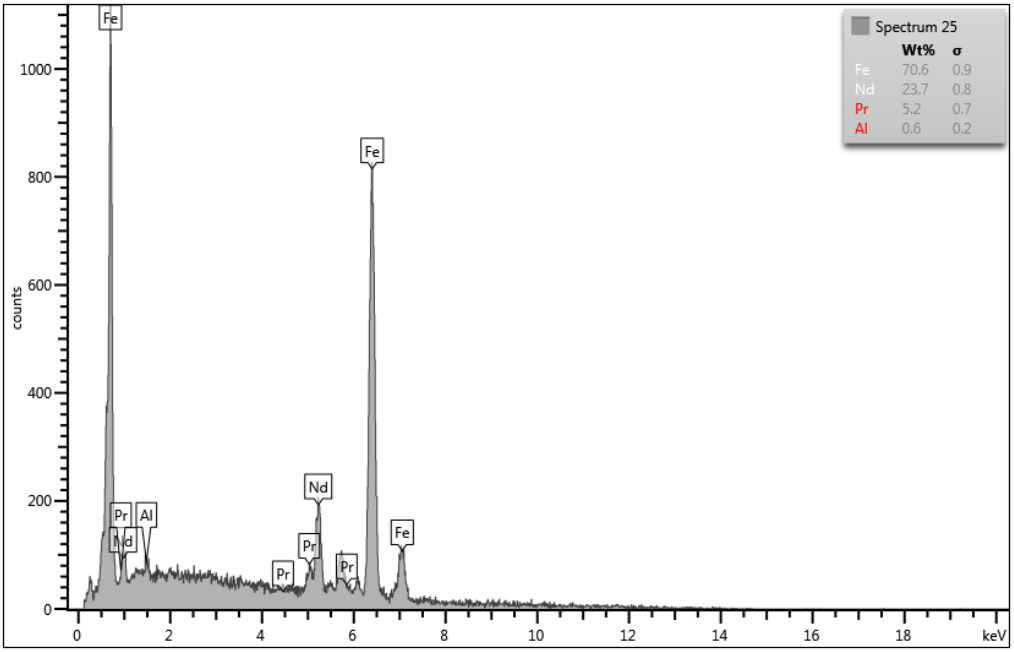

Figure 49 - Nd2Fe14B main phase spectrum.

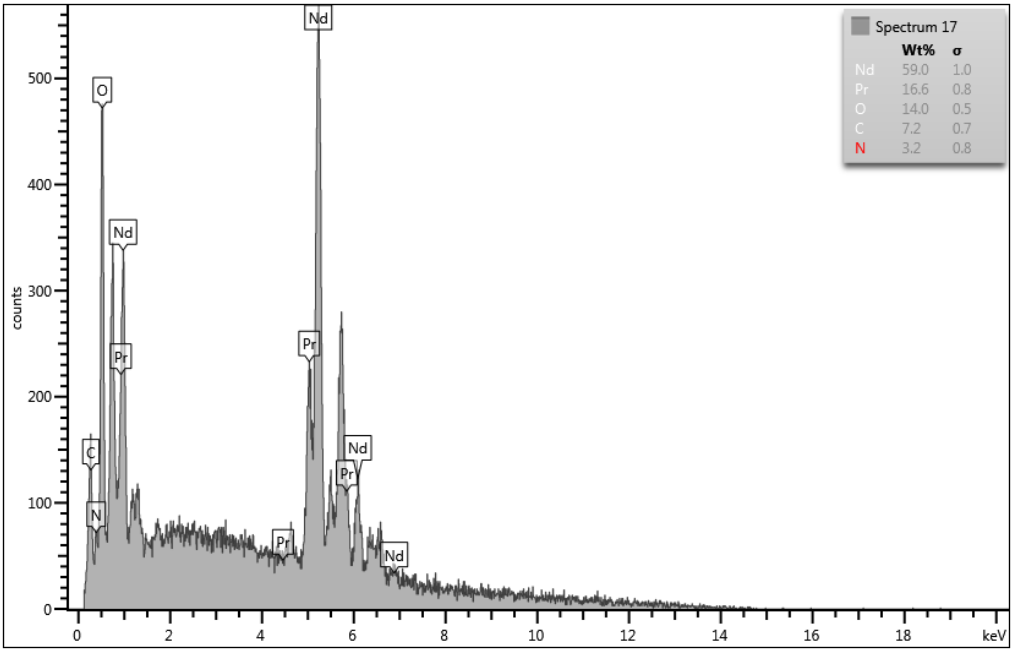

Figure 50 - Nd-Rich lighter areas.

The presence of the surface and subsurface defects presented in Figure 48 will be a problem for the magnet. The microcracks present in the surface and subsurface will result in stress generating points, which can lead to mechanical failure for the magnet. In addition, if the cracks meet, they can also lead to a

process called whole grain remove, which would be very detrimental for the part itself as well for the magnetic properties of the magnet since it would be losing magnetic material and nucleating reverse domains [57]. For an industrial application the surface and part of the subsurface would need to be removed in order to assure that all the defects in the surface and subsurface would be removed.

4.3.2 - Cross section layer for C822 semi-finishing machining condition

Since the semi-finishing and finishing conditions have less energy level during the machining, the effect on the surface and towards the bulk was less detrimental. Figure 51 shows a BSE image obtained with one thousand times magnification. It's possible to observe that the thickness of remolten material and spheres layer is much smaller than the one present previously. It is also possible to observe that the same texture towards the bulk composed of $Nd_2Fe_{14}B$ and Nd-rich areas is present for this sample.

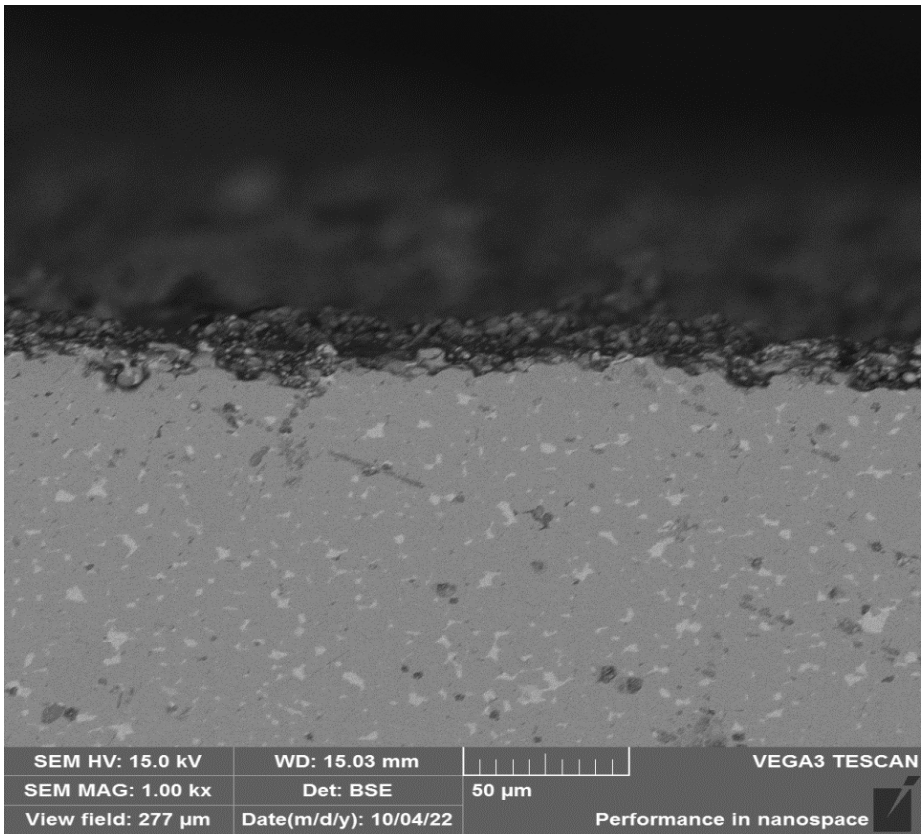

Figure 51 - Cross-sectional cut analysis for semi-finishing machining condition.

As it can be seen, it was not possible to observe the presence of subsurface microcracks, which is an indicator that this semi-finishing machining condition is not as aggressive for the subsurface as the roughing machining condition. In addition, it was also noticed a reduction in the presence of debris which is also an indicator that this machining condition did not damage so much the surface and the subsurface. Moreover, the surface above the subsurface looks more uniform when compared to the image presented for the roughing condition. It can be said that for this condition less material from the subsurface would needed to be removed when compared to the previous condition, however pos-processing would still be necessary to guarantee a surface and subsurface free from defects.

4.3.3 - Cross section layer for C823 and C824 finishing machining conditions

Since the last two conditions are really similar in parameters and results, the cross-sectional results for these two conditions will be displayed together in Figure 52. The stains contained in the picture do not reflect another chemical composition, they are craters that appeared due to sample preparation problems. In general, it's possible to expect a smaller impact on the magnetic properties for the samples machined with less aggressive conditions.

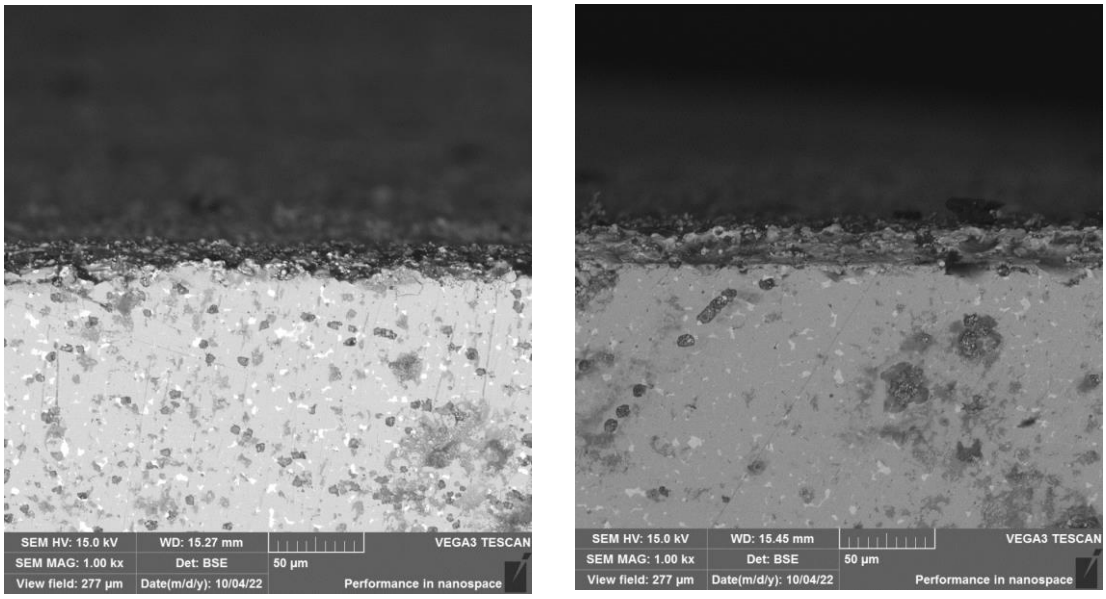

Figure 52 - Cross-sctional layer for finishing condition (left) C823 and (right) C824.

It’s possible to observe that there was also a reduction in microcracks in the subsurface, as well as a smaller debris formation for this last two finishing machining conditions. This last two conditions presented practically the same results for all the analysis that were made and presented in this work. As a result, they could be used interchangeably for an industrial application.

When comparing the roughing, semi-finishing and finishing conditions, it’s possible to say that the roughing condition damaged much more the subsurface, and therefore it would need a bigger material removal in a pos-processing operation, this would increase the waste of material. On the other hand, the finishing conditions had a smaller impact on surface and subsurface, however they still need pos-processing too. The disadvantage of the semi-finishing and finishing machining conditions would be that they have a slower material removal rate, it’s logical that a less energetic machining condition will also have a less material removal rate. Taking this in consideration, the choice between rough or finish machining conditions would depend on the application and the final objective of the manufactured magnet. Therefore, further specific study and also studies regarding the productivity would be necessary for deciding which condition makes more sense to be used in a real-life industrial application. What can be concluded is that the higher the energy input the higher it will be the damage on the surface, subsurface and the higher it will be the presence of surface and subsurface defects such as microcracks and debris.

4.4 – MAGNETIC PROPERTIES OF MACHINED SAMPLES

A VSM analysis was made in order to compare the properties of different Nd-Fe-B samples. The second quadrant of the hysteresis curve was treated according to the methodology described previously in order to compensate for the demagnetization fields. Samples machined with rough condition C821 (current = 7A, Time-On = 24 µs and Time-off = 14 µs) and the finishing condition C824 (current = 2.5A, Time-on = 31 µs and Time-off = 01 µs) were analysed. For each condition two different samples were studied. Figure 53 shows the two graphics, both for the more aggressive condition (blue curve) and for the finishing condition (orange curve). It is possible to observe that the magnetic properties such as coercivity and remanence were much more affected by the roughing

(C821) machining condition than the finishing condition (C824). The coercivity was reduced by approximately 30% for the sample machined by the roughing condition and remanence had a 27% reduction when comparing the results between the two conditions. Magnets applications require strict project requirements and any degrading on the magnet properties could compromise its application [59, 60].

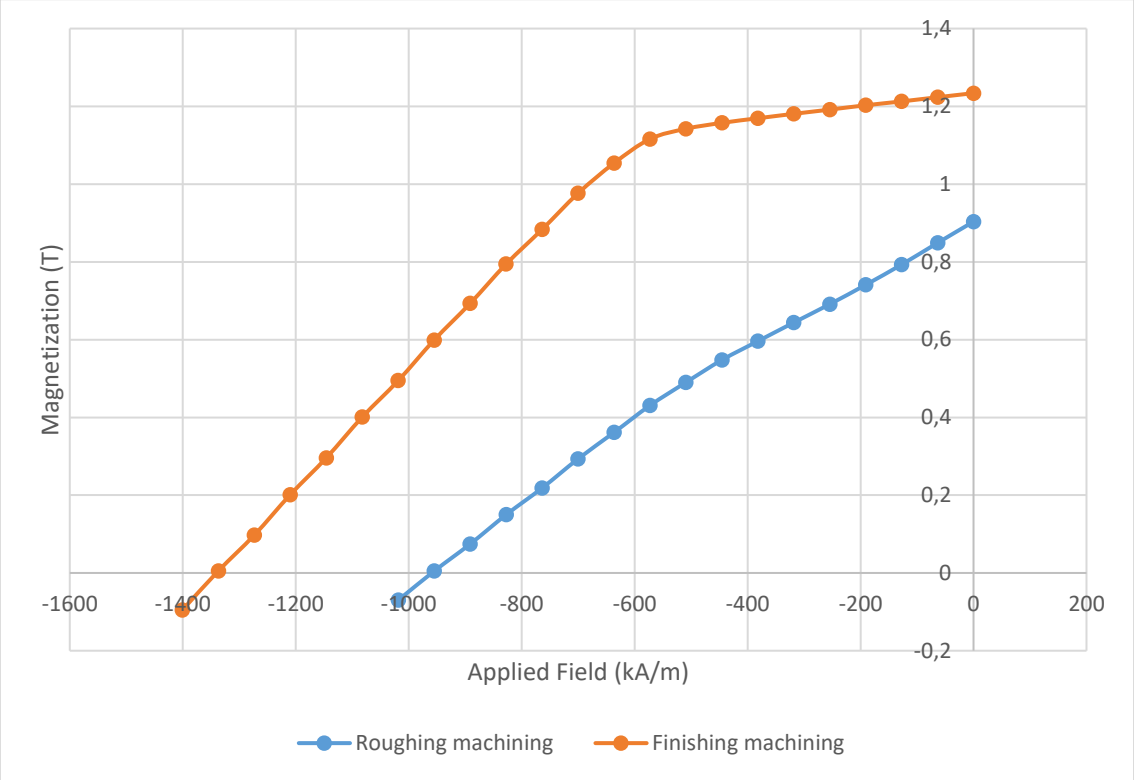

Figure 53 - Second quadrant magnetic properties.

Previously, it was shown that the rough machining had a consequence of big amount of disproportioned $Nd_2Fe_{14}B$ material into Fe and Nd/Pr dominant regions. Since Fe is a soft magnetic material, the samples machined with rough condition suffered a more intense magnetic softening phenomenon. Table 4 shows the values for coercivity and remanence obtained for the two samples. As it can be seen, the results for the finishing condition are much closer to standard N42 $Nd_2Fe_{14}B$ magnets values for coercivity and remanence [60], indicating that this machining condition was much less detrimental to the samples.

Table 4 -HcJ e B values for samples machined with rough and finishing machining conditions.

Condition	Roughing	Finishing
Remanence (T)	0.90	1.23
Coercivity (kA/m)	-954.68	-1336.73

In general, the experiments with wire electrical discharge machining have shown that the higher the energy input provided in the cutting zone, the higher it will be the detrimental effect on the surface, which in turn will have an influence on the magnetic properties. However, it was also shown in previous chapters that even for the finishing conditions there was a formation of a remelted layer, which was composed of distinct areas composed mainly by Nd and Fe. This means that even for the finishing conditions the use of pos-processing would be necessary in order to remove this remelted layer, which contains microcracks and debris that can lead to a mechanical failure of the magnet [61]. Next chapter will bring the conclusions made after studying all the results that were obtained in this work as well as future work suggestions to further study in such an interesting and important field such as machining of rare-earth elements with WEDM.

5 – CONCLUSIONS AND SUGGESTIONS FOR FUTURE WORKS

5.1 – CONCLUSIONS

This work analyzed the machining of a commercially available Nd-Fe-B wind turbine magnet machined by wire electrical discharge machining under rough, semi-finishing and finishing conditions. The main conclusions are the following:

- The first machining condition C821 (IP = 7 A, ON = 24 μs and OFF = 15 μs) presented results of roughness parameters (Ra, Rq, Rz and Rt) approximately 10 times higher than the last two conditions (considered as finishing conditions). In addition, the SEM images have shown a much more damaged surface, consisting of thick remolten material layer covered with unattached sphere-shaped chips. These chips indicate that the material was in a liquid state and solidified in this hollow or solid sphere format. These debris could have different chemical compositions, the first one believed to be made of neodymium oxide. The second composition is believed to be made of Fe-α due to its liberation during the discharging phenomena. Besides this layer, even given the very aggressive conditions, there was no observation of any considerably damage towards the bulk of the material.

- The second machining condition namely C822 is a semi-finishing machining condition. This condition produced roughness results three times higher when compared to the last two conditions and also three times smaller when compared to rough condition. Which makes this condition an intermediate condition regarding energy deliver and its effects on surface. Scanning electron microscope results, however, have shown that a sphere-shaped chip layer does not constitute this condition. Instead of that, this condition is made of a cracked remolten layer, having a mixed composition of Nd and Fe-α dominant areas.

- The last two conditions (C823 and C824) were very similar since the beginning, having the same almost the same value for current (2 A and 2.5 A respectively), Pulse On Time T_{on} equals to 31 μs and T_{off} = 31 μs for C823 and T_{off} = 01 μs for the last condition. The results for roughness were under a six per cent difference in absolute value. SEM and EDS results have shown also a remolten layer covering the whole surface, however it was not observed the presence of a chip layer. This remolten layer has also a mixed composition believed to be made of neodymium and Fe-α.

- The results of the screening tests for magnetic properties have shown a significant decrease in remanence and coercivity for the magnets machined with the roughing condition, in addition a magnetic softening phenomenon was also observed due to the segregation of Nd-Rich and Fe-α during the machining process. Since magnetization starts on the surface, it is believed that this impact on coercivity is due the chip layer that remained attached to the surface, which is composed of two main phases as previously discussed. Since one of these compositions is made of Fe-α, which can be considered as a soft magnetic phase, a decrease in HcJ values was expected. For the finishing condition the values of remanence and coercivity were closer to the reference values of remanence and coercivity for N42 class Nd-Fe-B magnets, indicating that this condition didn't have the same intensity of magnetic damaged when compared to the roughing condition.

- In general, it is possible to conclude that wire electrical discharge machining can be a suitable machining process for the manufacturing of rare-earth based magnets. The more aggressive the condition, the more negative effects it will be observed on its surface roughness, and which in turns will have a significant potential magnetic damage effect on its magnetic properties at least for small samples. In any case, further post processing, like grinding for example, is needed on the manufacturing of

Nd-Fe-B magnets in order to remove the remolten layer present on its surface.

5.2 – WORK SUGGESTIONS

The following suggestions for further studies are based on the opportunities and difficulties felt during this work:

- Evaluate the possibility of the creation of wire electrical discharge machining parameters in order to minimize the damage on the surface;
- Thermal simulation of the discharging process for a defined geometry in order to understand better the chip formation phenomena;
- The machining of bigger magnets with the same machining conditions, but evaluating magnetic properties with a closed loop measurement;
- Evaluation of particle size, chemical composition and magnetic properties of chip generated by the machining of Nd-Fe-B magnets with WEDM;
- The manufacturing of magnets with these chips generated by WEDM.

6 – REFERENCES

[1] BRADLEY S. VAN GOSEN. **Critical mineral resources of the United States— Economic and environmental geology and prospects for future supply**. Reston: U.S. Geological Survey, 2017. 44 p.

[2] BRADLEY S. VAN GOSEN. **Rare Earth Mineral Deposits in the United States**. Reston: U.S. Geological Survey, 2019. 24 p.

[3] LYDIA MARIA LOBATO. **Recursos minerais no cenário geológico de Minas Gerais.** CODEMGE, 2018. 77p.

[4] KLOCKE, F., **Manufacturing Processes 1**, vol. 101, no. 5. Berlin, Heidelberg: Springer Berlin Heidelberg, 2011.

[5] ICHIMURA, Yoshihiro *et al*. Relationship between Magnetic Flux Density and Temperature Distributions of Permanent Magnets by EDM. **Key Engineering Materials**, [S.L.], v. 523-524, p. 322-327, nov. 2012. Trans Tech Publications, Ltd.. http://dx.doi.org/10.4028/www.scientific.net/kem.523-524.322.

[6] Weingaertner, W. – Gedankenexperiment about the phenomena governing an electrical discharge between two electrodes in metal removal process by electrical discharge**. 15th MIC - Conferência de inovações em usinagem para a indústria aeroespacial**. Hannover, 2015.

[7] KLOCKE, F.; KÖNIG, W., Fertigungsverfahren 3. Berlin, Heidelberg: Springer Berlin Heidelberg, 2007.

[8] AMORIM, Fred Lacerda; WEINGAERTNER, Walter Lindolfo; BASSANI, Irionson Antonio. Aspects on the optimization of die-sinking EDM of tungsten carbide-cobalt. **Journal Of The Brazilian Society Of Mechanical Sciences And Engineering**, [S.L.], v. 32, n. , p. 496-502, dez. 2010. Springer Science and Business Media LLC. http://dx.doi.org/10.1590/s1678-58782010000500009.

[9] LUZIA, Cezar Augusto Oleinik *et al*. Recast layer mechanical properties of tool steel after electrical discharge machining with silicon powder in the dielectric. **The International Journal Of Advanced Manufacturing Technology**, [S.L.], v. 103, n. 1-4, p. 15-28, 13 mar. 2019. Springer Science and Business Media LLC. http://dx.doi.org/10.1007/s00170-019-03549-w.

[10] RIFFEL, Germano. **Influência da fenda de trabalho e da lavagem nas condições de operação da eletroerosão por faísca**. 1992. 127 f. Dissertação (Mestrado) - Curso de Engenharia Mecânica, Centro Tecnológico, Universidade Federal de Santa Catarina, Florianópolis, 1992.

[11] PALANIKUMAR, K.; DAVIM, J. Paulo. Electrical discharge machining: study on machining characteristics of wc/co composites. **Machining And Machine-Tools**, [S.L.], p. 135-168, 2013. Elsevier. http://dx.doi.org/10.1533/9780857092199.135.

[12] CROAT, John. **HIGH COERCIVITY RARE EARTH-IRON MAGNETS**. Titular: General Motors. US n. 4,496,395. Depósito: 26 out. 1981. Concessão: 07 fev. 1989.

[13] HERBST, J. F.; CROAT, J. J.; YELON, W. B.. Structural and magnetic properties of Nd2Fe14B (invited). **Journal Of Applied Physics**, [S.L.], v. 57, n. 8, p. 4086-4090, 15 abr. 1985. AIP Publishing. http://dx.doi.org/10.1063/1.334680.

[14] HONO, K.; SEPEHRI-AMIN, H.. Strategy for high-coercivity Nd–Fe–B magnets. **Scripta Materialia**, [S.L.], v. 67, n. 6, p. 530-535, set. 2012. Elsevier BV. http://dx.doi.org/10.1016/j.scriptamat.2012.06.038.

[15] CARVALHO, Matheus. **Metodologia de obtenção de ímãs à base de Nd-Fe-B via moldagem de pós por injeção**. 2013. 102 f. Dissertação (Mestrado) - Curso de Engenharia Mecânica, Centro Tecnológico, Universidade Federal de Santa Catarina, Florianópolos, 2013.

[16] MCGUINESS, P. J.; DEVLIN, E.; HARRIS, I. R.; ROZENDAAL, E.; ORMEROD, J.. A study of Nd-Fe-B magnets produced using a combination of hydrogen decrepitation and jet milling. **Journal Of Materials Science**, [S.L.], v. 24, n. 7, p. 2541-2548, jul. 1989. Springer Science and Business Media LLC. http://dx.doi.org/10.1007/bf01174525.

[17] CHENG, C.W.; MAN, H.C.; CHENG, F.T.. Magnetic and corrosion characteristics of Nd-Fe-B magnet with various surface coatings. **Ieee Transactions On Magnetics**, [S.L.], v. 33, n. 5, p. 3910-3912, 1997. Institute of Electrical and Electronics Engineers (IEEE). http://dx.doi.org/10.1109/20.619612.

[18] WENDHAUSEN, Paulo. **Tecnologia de produção de ímãs SmCo5**. 1990. 112 f. Dissertação (Mestrado) - Curso de Engenharia Mecânica, Centro Tecnólogico, Universidade Federal de Santa Catarina, Florianópolis, 1990.

[19] LIU, Wei; WU, Jiansheng. Mechanical properties and fracture mechanism study of sintered Nd–Fe–B alloy. **Journal Of Alloys And Compounds**, [S.L.], v. 458, n. 1-2, p. 292-296, jun. 2008. Elsevier BV. http://dx.doi.org/10.1016/j.jallcom.2007.04.277.

[20] LI, Li; QI, Li Ling; ZHAI, Xiao Qing; WANG, Dong. Surface Modification by Electrical Discharge Machining of Sintered NdFeB Magnet. **Advanced Materials Research**, [S.L.], v. 139-141, p. 390-393, out. 2010. Trans Tech Publications, Ltd.. http://dx.doi.org/10.4028/www.scientific.net/amr.139-141.390.

[21] LI, Li; NIU, Zong Wei; YIN, Feng Shi; LIU, Yuan Yong. Surface Integrity of Sintered NdFeB Permanent Magnet after EDM. **Advanced Materials Research**, [S.L.], v. 503-504, p. 27-30, abr. 2012. Trans Tech Publications, Ltd.. http://dx.doi.org/10.4028/www.scientific.net/amr.503-504.27.

[22] LI, Li; NIU, Zong Wei; ZHANG, Jian Hua. Investigation of Material Removal Mechanism in EDM of Sintered NdFeB Permanent Magnet. **Key Engineering Materials**, [S.L.], v. 334-335, p. 937-940, mar. 2007. Trans Tech Publications, Ltd.. http://dx.doi.org/10.4028/www.scientific.net/kem.334-335.937.

[23] KIM, H. T.; KIM, Y. B.; KAPUSTIN, G. A.. Effects of machining on the magnetic properties of sintered NdFeB magnets. **Physica Status Solidi (A)**, [S.L.], v. 201, n. 8, p. 1913-1916, jun. 2004. Wiley. http://dx.doi.org/10.1002/pssa.200304621.

[24] TANG, Weizhong; ZHOU, Shouzeng; WANG, Run. On the neodymium-rich phases in Nd-Fe-B magnets. **Journal Of The Less Common Metals**, [S.L.], v. 141, n. 2, p. 217-223, ago. 1988. Elsevier BV. http://dx.doi.org/10.1016/0022-5088(88)90407-9.

[25] B. C. Dodrill, B. J. Kelley. **Measurements with a VSM – Permanent Magnet Materials.** Westernville, OH: Lake Shore Cryotronics.:. 1999. 6 p.

[26] Bozorth, Richard M. **Ferromagnetism.** New Jersey: IEEE, 1993. 992 p.

[27] Callister, William D. **Materials Science and Engineering - Introduction.** Utah**:** Willey 1994. 992 p.

[28] Jiles, D. **Introduction to Magnetism and Magnetic Materials**. London: Chapman and Hall1998. 626 p.

[29] SILVA, Melissa. **WENDHAUSEN, Paulo. Tecnologia de produção de ímãs SmCo5. 1990. 112 f. Dissertação (Mestrado) - Curso de Engenharia Mecânica, Centro Tecnólogico, Universidade Federal de Santa Catarina, Florianópolis, 1990.** 20017. 96 f. Dissertação (Mestrado) - Curso de Engenharia de Materiais, Instituto de Pesquisas Energéticas e Nucleares, São Paulo, 2017.

[30] Willian F. Brown, Jr. Virtues and Weaknesses of the Domain concept. **Reviews of Modern Physics.** vol. 17, p. 15 – 20. jan. 1945.

[31] SCOTT, D. W.; MA, B. M.; LIANG, Y. L.; BOUNDS, C. O.. Microstructural control of NdFeB cast ingots for achieving 50 MGOe sintered magnets. **Journal Of Applied Physics**, [S.L.], v. 79, n. 8, p. 4830-4832, 15 abr. 1996. AIP Publishing. http://dx.doi.org/10.1063/1.361622.

[32] B. Ebenhard. Development of a precision, low-cost, small foorpint wire electron discharge machine (WEDM). **Proceedings of the American Society for Precision Engineering Conference. jan.** 2006.

[33] GF AgieCharmilles. **User Manual: CUT 20P – CUT 30 P**. Basis – Original Instructions – Id. N° 500.080.754, 2012.

[34] MILLER, Scott F.; KAO, Chen-C.; SHIH, Albert J.; QU, Jun. Investigation of wire electrical discharge machining of thin cross-sections and compliant mechanisms. **International Journal Of Machine Tools And Manufacture**, [S.L.], v. 45, n. 15, p. 1717-1725, dez. 2005. Elsevier BV. http://dx.doi.org/10.1016/j.ijmachtools.2005.03.003.

[35] Jameson, E. C. **Electrical discharge machining.** Michigan: Elman C. Jameson and Society of manufacturing engineers**,**. 2001. 329 p.

[36] Fleming, B. **The EDM How-to book.** Fleming publications. 2005. 155 p.

[37] TaylorSurf il20. **Operator's Handbook.** Taylor Surf.

[38] **International organization for standardization. ISO 4287:2008.** Geometrical Product Specifications (GPS) – Surface texture: Profile method – Terms, definitions and surface texture parameters.

[39] Hitachi Tabletop Microscope TM3030**. User manual and specifications**.

[40] RAVAUD, Romain; LEMARQUAND, Guy. MAGNETIC FIELD PRODUCED BY A PARALLELEPIPEDIC MAGNET OF VARIOUS AND UNIFORM POLARIZATION. **Progress In Electromagnetics Research**, [S.L.], v. 98, p. 207-219, 2009. The Electromagnetics Academy. http://dx.doi.org/10.2528/pier09091704.

[41] CHEN, Du-Xing; PARDO, E.; SANCHEZ, A.. Demagnetizing factors of rectangular prisms and ellipsoids. **Ieee Transactions On Magnetics**, [S.L.], v. 38, n. 4, p. 1742-1752, jul. 2002. Institute of Electrical and Electronics Engineers (IEEE). http://dx.doi.org/10.1109/tmag.2002.1017766.

[42] CARLINI, Giovani. **Remoção de metal duro por EDM com eletrodo de CuW**. 2018. 113 f. Dissertação (Mestrado) - Curso de Engenharia Mecânica, Centro Tecnológico, Universidade Federal de Santa Catarina, Florianópolis, 2018.

[43] KUNIEDA, Masanori; FURUDATE, Chika. High Precision Finish Cutting by Dry WEDM. **Cirp Annals**, [S.L.], v. 50, n. 1, p. 121-124, 2001. Elsevier BV. http://dx.doi.org/10.1016/s0007-8506(07)62085-x.

[44] G. Wit, K. Bodgan, R. Adam. Surface integrity of Machined Surfaces **Springer.** London**.** p. 143 – 179**.** 2010.

[45] Jeremy Greer. Wire Electrical Discharge Machining of Helical Devices from Permanent Magnets**. 2011. 88 f. Tese (Doutorado). Departamento de Engenharia Mecânica, Universidade de Utah.**

[46] NAVARRO, F. Hernández *et al*. Influence of chemical composition and processing conditions on the microstructure and magnetic properties of low-carbon Si-Al-Sb electrical steel sheets. **Journal Of Magnetism And Magnetic Materials**, [S.L.], v. 569, p. 170431, mar. 2023. Elsevier BV. http://dx.doi.org/10.1016/j.jmmm.2023.170431.

[47] LANDGRAF, Fernando José Gomes; SILVEIRA, João Ricardo Filipini da; RODRIGUES-JR., Daniel. Determining the effect of grain size and maximum induction upon coercive field of electrical steels. **Journal Of Magnetism And Magnetic Materials**, [S.L.], v. 323, n. 18-19, p. 2335-2339, out. 2011. Elsevier BV. http://dx.doi.org/10.1016/j.jmmm.2011.03.034.

[48] WOODCOCK, T.G. *et al*. Understanding the microstructure and coercivity of high performance NdFeB-based magnets. **Scripta Materialia**, [S.L.], v. 67, n. 6, p. 536-541, set. 2012. Elsevier BV. http://dx.doi.org/10.1016/j.scriptamat.2012.05.038.

[49] REOLON, Luca Watanabe *et al*. WEDM performance and surface integrity of Inconel alloy IN718 with coated and uncoated wires. **The International Journal Of Advanced Manufacturing Technology**, [S.L.], v. 100, n. 5-8, p. 1981-1991, 12 out. 2018. Springer Science and Business Media LLC. http://dx.doi.org/10.1007/s00170-018-2828-6.

[50] MORITZ, Pierre *et al*. Development Of Micro-Magnets For The Electromagnetic Transduction Of MEMS. **2019 20Th International Conference On Solid-State Sensors, Actuators And Microsystems & Eurosensors Xxxiii (Transducers & Eurosensors Xxxiii)**, [S.L.], p. 10-20, jun. 2019. IEEE. http://dx.doi.org/10.1109/transducers.2019.8808335.

[51] GUTFLEISCH, Oliver *et al*. Magnetic Materials and Devices for the 21st Century: stronger, lighter, and more energy efficient. **Advanced Materials**, [S.L.], v. 23, n. 7, p. 821-842, 15 dez. 2010. Wiley. http://dx.doi.org/10.1002/adma.201002180.

[52] LI, Z. B. *et al*. Nucleation of reversed domain and pinning effect on domain wall motion in nanocomposite magnets. **Applied Physics Letters**, [S.L.], v. 103, n. 6, 5 ago. 2013. AIP Publishing. http://dx.doi.org/10.1063/1.4817968.

[53] BERNARDI, J.; FIDLER, J.; SAGAWA, M.; HIROSE, Y.. Microstructural analysis of strip cast Nd–Fe–B alloys for high (BH)max magnets. **Journal Of Applied Physics**, [S.L.], v. 83, n. 11, p. 6396-6398, 1 jun. 1998. AIP Publishing. http://dx.doi.org/10.1063/1.367557.

[54] Griffiths, B. **Manufacturing Surface Technology**.. London: Penton Press, 2001. 256 p.

[55] M'SAOUBI;, R. *et al*. A review of surface integrity in machining and its impact on functional performance and life of machined products. **International Journal Of Sustainable Manufacturing**, [S.L.], v. 1, n. 1/2, p. 203, 2008. Inderscience Publishers. http://dx.doi.org/10.1504/ijsm.2008.019234.

[56] PADILHA, Angelo Fernando. **Técnicas de Análise Microestrutural**. Hemus, 2006. 192 p.

[57] SUZUKI, Toshimasa *et al*. Direct Observation of Reverse Magnetic Domain and Magnetic Domain Wall Motion in Nd-Fe-B Magnet at High Temperature by Lorentz Microscop. **Mrs Advances**, [S.L.], v. 1, n. 3, p. 241-246, jan. 2016. Springer Science and Business Media LLC. http://dx.doi.org/10.1557/adv.2016.29.

[58] HALL, Michael. International comparison of the properties of NdFeB permanent magnets measured using an electromagnet and a pulsed field magnetometer. **Journal Of The Korean Physical Society**, [S.L.], v. 63, n. 3, p. 726-728, ago. 2013. Korean Physical Society. http://dx.doi.org/10.3938/jkps.63.726.

[59] TANG, Weizhong; ZHOU, Shouzeng; WANG, Run. On the neodymium-rich phases in Nd・Fe・B magnets. **Journal Of The Less Common Metals**, [S.L.], v. 141, n. 2, p. 217-223, ago. 1988. Elsevier BV. http://dx.doi.org/10.1016/0022-5088(88)90407-9.

[60] MA, B. M.; BOUNDS, C. O.. The impact of the directional solidification on the magnetic properties of NdFeB magnets. **Journal Of Applied Physics**, [S.L.], v. 70, n. 10, p. 6471-6473, 15 nov. 1991. AIP Publishing. http://dx.doi.org/10.1063/1.349934.